

## **Durham Research Online**

# Deposited in DRO:

26 June 2018

#### Version of attached file:

Accepted Version

#### Peer-review status of attached file:

Peer-reviewed

# Citation for published item:

Perri, Edoardo and Tucker, Maurice E. and Słowakiewicz, Mirosław and Whitaker, Fiona and Bowen, Leon and Perrotta, Ida D. (2018) 'Carbonate and silicate biomineralization in a hypersaline microbial mat (Mesaieed sabkha, Qatar): roles of bacteria, extracellular polymeric substances and viruses.', Sedimentology., 65 (4). pp. 1213-1245.

#### Further information on publisher's website:

https://doi.org/10.1111/sed.12419

## Publisher's copyright statement:

This is the accepted version of the following article: Perri, Edoardo, Tucker, Maurice E., Słowakiewicz, Mirosław, Whitaker, Fiona, Bowen, Leon Perrotta, Ida D. (2018). Carbonate and silicate biomineralization in a hypersaline microbial mat (Mesaieed sabkha, Qatar): Roles of bacteria, extracellular polymeric substances and viruses. Sedimentology 65(4): 1213-1245 which has been published in final form at https://doi.org/10.1111/sed.12419. This article may be used for non-commercial purposes in accordance With Wiley Terms and Conditions for self-archiving.

#### Additional information:

## Use policy

The full-text may be used and/or reproduced, and given to third parties in any format or medium, without prior permission or charge, for personal research or study, educational, or not-for-profit purposes provided that:

- $\bullet\,$  a full bibliographic reference is made to the original source
- a link is made to the metadata record in DRO
- $\bullet \,$  the full-text is not changed in any way

The full-text must not be sold in any format or medium without the formal permission of the copyright holders.

Please consult the full DRO policy for further details.

DR. EDOARDO PERRI (Orcid ID: 0000-0001-9825-7098)

Article type : Original Manuscript

Corresponding author mail id:- eperri@unical.it

Carbonate and silicate biomineralization in a hypersaline microbial mat (Mesaieed sabkha, Qatar): Roles of bacteria, extracellular polymeric substances and viruses

Edoardo Perri<sup>\*</sup>, Maurice E. Tucker<sup>† ‡</sup>, Mirosław Słowakiewicz<sup>‡ §</sup>, Fiona Whitaker<sup>† ‡</sup>, Leon Bowen<sup>¶</sup> and Ida D. Perrotta<sup>\*</sup>

#### Associate Editor - Giovanna Della Porta

## Short title – Biomineralization of a hypersaline microbial mat

#### **ABSTRACT**

In a modern peritidal microbial mat from Qatar, both biomediated carbonates and Mg-rich clay minerals (palygorskite) were identified. The mat, ca 5 cm thick, shows a clear lamination reflecting different microbial communities. The initial precipitates within the top millimetres of the mat are composed of Ca-Mg-Si-Al-S amorphous nanoparticles (few tens of nanometres) that replace the ultrastructure of extracellular polymeric substances. The extracellular polymeric substances are enriched in the same cations and act as a substrate for mineral nucleation. Successively crystallites of palygorskite fibres associated with carbonate nanocrystals develop, commonly surrounding bacterial bodies. Micron-sized crystals of low-Mg calcite are the most common precipitates, together with subordinate aragonite, very high-Mg calcite/dolomite and ankerite. Pyrite nanocrystals and framboids are present in the deeper layers of the mat. Calcite crystallites form conical structures, circular to triangular/hexagonal in cross-section, evolving to crystals with rhombohedral terminations; some crystallite bundles develop into dumb-bell and stellate forms. Spheroidal organo-mineral structures are also common within the mat. Nanospheres, a few tens of nanometres in diameter, occur attached to coccoid bacteria and within their cells; these are interpreted as permineralized viruses, and could be significant as nuclei for crystallite-crystal precipitation. Microspheres, 1 to 10 µm in diameter, result from intracellular permineralization within bacteria or the mineralization of the bacteria themselves. Carbonates and clay minerals are commonly This article has been accepted for publication and undergone full peer review but has not been through the copyediting, typesetting, pagination and proofreading process, which may lead to differences between this version and the Version of Record. Please cite this article as doi: 10.1111/sed.12419

<sup>\*</sup>Dipartimento di Biologia Ecologia e Scienze della Terra, Università della Calabria, Via P. Bucci Cubo 15b, 87036 Rende, Italy

<sup>&</sup>lt;sup>†</sup>School of Earth Sciences, University of Bristol, BS8 1RJ, UK

<sup>‡</sup>Cabot Institute, University of Bristol, Cantock's Close, Bristol BS8 1UJ, UK

<sup>§</sup> Organic Geochemistry Unit, School of Chemistry, University of Bristol, Cantock's Close BS8 1TS, UK

<sup>&</sup>lt;sup>¶</sup>Department of Physics, Durham University, DH1 3LE, UK

aggregated to form peloids, tens of microns in size, surrounded by residual organic matter. Magnesium-silicate and carbonate precipitation are likely to have been driven by pH – saturation index – redox changes within the mat, related to micro-environmental chemical changes induced by the microbes – extracellular polymeric substances – viruses and their degradation.

**Keywords**: Bacteria, biomediated carbonate, biomediated clay, EPS, microbial mat, nanospheres, viruses

#### INTRODUCTION

In the last few years there has been increasing interest in the role of microbes in the precipitation of carbonate minerals and others including clay minerals, iron compounds and phosphates. In particular there has been a focus on the possibility of microbes being involved in the precipitation of dolomite (see Kaczmarek et al., 2017, and references cited therein) and these studies have particularly involved modern microbial mats (e.g. Dupraz et al., 2009). Microbial mats develop under a wide range of environmental conditions at the present time and they have played a significant role in the development of organosedimentary deposits (microbialites; Burne & Moore, 1987) that record the early history of life on Earth (Grotzinger & Knoll, 1999; Hofmann et al., 1999; Van Kranendonk et al., 2008; Nutman et al., 2016). The characteristic continuous to wavy lamination of microbial mats develops from interacting microbial communities, which by their upward growth and EPS (extracellular polymeric substances) trap and embed sediment grains, precipitate new minerals, and eventually through lithification produce laminated (stromatolites), clotted/unlaminated (thrombolites) and concentric (oncolites) varieties of microbialite (Canfield & Des Marais, 1993; Wingender et al., 1999; Allison et al., 2000; Riding, 2000; Decho et al., 2005; Dupraz et al., 2009).

The presence of EPS, a term that refers to all organic molecules secreted by microbes and that constitute most of the biomass of microbial mats (Characklis & Wilderer, 1989; Decho, 1990; Staudt *et al.*, 2004), probably plays the key role in the mineralization process although the exact mechanisms are not yet resolved. For instance, EPS, which consist of an organic matrix with anionic functional groups, are capable of binding metal ions such as Ca<sup>2+</sup> and Mg<sup>2+</sup> (Reitner & Neuweiler, 1995; Braissant *et al.*, 2007). When microbial enzymes degrade EPS, the cations are liberated and carbonate minerals may precipitate (Dupraz & Visscher, 2005; Glunk *et al.*, 2011). Specifically, the metabolic reactions of cyanobacteria and sulphate-reducing bacteria appear to promote the precipitation of aragonite, calcite, monohydrocalcite, vaterite, high-Mg calcite, very high-Mg calcite/dolomite, magnesite,

gypsum and/or silicate minerals (Lyons *et al.*, 1984; Thompson & Ferris, 1990; Tazaki, 1997; Ludwig *et al.*, 2005; Vasconcelos *et al.*, 2006; Kremer *et al.*, 2008; Paulo & Dittrich, 2013; Bontognali *et al.*, 2014; Burne *et al.*, 2014; Zeyen *et al.*, 2015; Brauchli *et al.*, 2016; Pace *et al.*, 2016). These mineral precipitates exhibit a range of morphologies, including rhombs, dumb-bells, needles and spheroids.

In addition to bacteria and EPS, potentially of greater significance in terms of mineral precipitation, but difficult to prove, is the presence of viruses within microbial mats (Pacton *et al.*, 2014; De Wit *et al.*, 2015). Viruses are present in all other modern environments as well (see Suttle, 2013), including the subsurface; for example, down to several 100 m in granitic rocks (Kyle *et al.*, 2008a) and they are likely to be present on Mars as well (Griffin, 2013). Viruses are everywhere in superabundance; whereas a millilitre of seawater may contain millions of bacteria (10<sup>6</sup>), there are likely to be tens of millions to a billion viruses there as well (10<sup>7</sup> to 10<sup>9</sup>/ml; Suttle, 2007). There are equally huge numbers within near-surface sediments and microbial mats (for example, 10<sup>8</sup> to 10<sup>10</sup> per cubic cm or gm; Carreira *et al.*, 2015).

Intertidal mesohaline microbial mats at Mesaieed in south-east Qatar (Fig. 1) help to shed light on the biomineralization processes in hypersaline microbially-dominated environments. These mats have been previously examined using microbiological, organic and inorganic geochemical methods, to provide insight into the very early diagenetic processes associated with the degradation of organic matter by sulphate reduction and methanogenesis (Słowakiewicz *et al.*, 2016).

The aim of this paper is to understand the role of the organic components of the mat (virus-like particles, micro-organisms and EPS) in the formation of the carbonate and silicate minerals. To analyse the mechanisms of neo-formed mineral nucleation and development in the mat, a multi-scale study was conducted. This has demonstrated the biogenic mediated origin of the autochthonous minerals after the key-role of the EPS and virus-like particles, in both accumulating cations and furnishing sites of nucleation. As a consequence, many species of carbonate minerals form within the mat, together with autochthonous biomediated Mg-rich clay minerals. Many new features relating to organic-matter; fluid interaction and mineral precipitation are described and interpreted here, relevant to the origin of microbialitic rocks.

# ENVIRONMENTAL SETTING AND MICROBIOLOGY OF THE MICROBIAL MAT

The Mesaieed sabkha is situated in southeast Qatar, to the south of Al-Wakrah (Fig. 1). Warm winters and very hot and humid summers characterize the area, with a mean daily temperature of 30 to 35°C and maximum surface temperature *ca* 50°C; mean rainfall is 77 mm yr<sup>-1</sup>, but this mostly occurs as rare high-intensity events, with the result that the area is extremely arid most of the time (Słowakiewicz *et al.*, 2014, 2016). The dominant north-west Shamal wind brings fine siliciclastic particles and detrital carbonate (mainly shell fragments and pedogenic grain coatings) across the sabkha. Seaward, a system of chenier beaches (Fig. 1A) that protects low-energy lagoons and ponds typifies the coast (Strohmenger & Jameson, 2015). In the Mesaieed area lagoons are typically narrow (100 to 500 m), elongate parallel to the coastline, and connected with the sea via narrow inlets with tidally-reversing currents (Fig. 1A and B). Metre-scale ponds, located more distant from the tidal inlets, are flooded less frequently (Słowakiewicz *et al.*, 2016).

Restriction of seawater circulation and high evaporation rates give rise to seasonal variations in salinity. Within the lagoons the salinity varies spatially, with complex temporal patterns at a range of scales (Whitaker *et al.*, 2014).

The lagoons are fringed by low-growing halophytic vegetation, climaxing in the development of narrow bands of mangrove (*Avicennia* sp.) near the top of the intertidal zone (Fig. 1A to C). The low-relief surface of the lagoon is mantled by dark-coloured laminated microbial mats. The mats are best developed in the middle to upper intertidal zone within ponded areas, between shallow tidal channels. The mats, which are typically 4 to 6 cm thick, are broken up into polygons, the edges of which are upturned, tufted and darker in colour (Fig. 1B to D). The mats develop upon carbonate muds containing bioclasts that make a transition to the siliciclastic—carbonate sediment below (Fig. 2).

Previous microbiological and molecular studies showed that the Mesaieed mat is characterized by a strong vertical zonation of bacteria and archaea resulting from interactions between the steep physiochemical gradients and physiology of the micro-organisms (Al-Thani *et al.*, 2014; Słowakiewicz *et al.*, 2016). The mat biomass is dominated by Proteobacteria (predominant in all layers and represented by Alphaproteobacteria, Deltaproteobacteria, Gammaproteobacteria), Halobacteria (abundant in all layers) and Chloroflexus (abundant in the middle layers), with subordinate Cyanobacteria (most abundant in the surficial layer) and Thaumarchaeota (abundant in the deepest layer) (Fig. 2).

Allochthonous biomass components are represented by *Halodule* seagrass, dinoflagellates and other algal communities.

#### **METHODS**

#### Sampling collection and preparation

Two representative mat samples were collected from holes dug within the intertidal zone of the restricted back-barrier coastal lagoon ponds at a location ca 2 km north-east of Mesaieed (Fig. 1; N 25°3'3.29" E 51°36'41.82"). Mat samples were frozen immediately after collection and kept frozen in transit to the University of Bristol and later to the Università della Calabria. Samples were subsequently defrosted prior to analysis.

## **Electron microscopic examination**

Scanning electron microscopic (SEM) examinations of fresh surfaces of the various layers of the microbial mat were carried out using a FEI-Philips ESEM-FEG Quanta 200F (Thermo Fisher Scientific, Waltham, MA, USA) at the Università della Calabria. For high-vacuum SEM observations, samples were fixed in 3% glutaraldehyde, post-fixed in OsO<sub>4</sub>, dehydrated in graded ethanol solutions and subsequently transferred to 100% HMDS with the same procedure using a series of ethanol–HMDS mixtures. During SEM observations, semi-quantitative analyses of micron-sized spots were performed by an EDAX Genesis 4000 energy-dispersive X-ray spectrometer (EDS) (EDAX, Mahwah, NJ, USA) operating at 20 kV with a working distance of 12 mm.

For routine transmission electron microscopy (TEM), all specimens were fixed in 3% glutaraldehyde (0.1 M phosphate buffer, pH 7.4), post-fixed in osmium tetroxide (3%), dehydrated in graded acetone solutions and embedded in Araldite epoxy resin (Fluka, Buchs, Switzerland). Ultrathin sections were prepared using a glass knife, collected on copper grids (G 300 Cu), and then examined with a JEOL JEM 1400 Plus (JEOL, Tokyo, Japan) instrument operating at 80 kV. EDS analysis was performed in the STEM mode at 80 kV accelerating voltage. Selected area diffraction (SAED) patterns were recorded using a selected area aperture 2 µm in diameter.

A parcel of each layer was prepared for further SEM observation at Durham University using a JEOL SEM 5600 LV, by first dissolving out the organic matter using a 10 to 15% concentration of sodium hypochlorite (bleach). The residue was shaken and after a few seconds, when the coarser material had settled to the bottom of the beaker, a small piece of glass (2 cm<sup>2</sup>) on a wire frame was lowered into the beaker and the material still in suspension

was allowed to settle on the glass. After 15 min, when the solution was clear, the glass was removed. The particles on the glass were all  $\leq 5 \mu m$ .

## X-ray diffraction (XRD) analysis

All powdered mat samples were analysed with XRD at the University of Bristol (Powder XRD D8 Advance; Bruker, Billerica, MA, USA) to determine the mineralogy, with one extracted sample run on a Phillips PW3710 X-ray diffractometer (PANalytical, Almelo, The Netherlands) at Oklahoma State University.

## **Hydrochemical analysis**

Measurements of specific electrical conductance (SEC, ±0.1 mS cm<sup>-1</sup>), pH (±0.01), temperature (±0.1°C) and dissolved O<sub>2</sub> (±0.1%) for the lagoon water overlying the mat were taken using a Hach's multi-parameter instrument kit and measured in the wall of the pits. Subsurface characterization of pore water was obtained with measurements at 1 cm depth intervals through the mat in each of the pits, and into the underlying sediment to a maximum depth of 15 cm. Salinity (PSU) was approximated from SEC using the relationship of Fofonoff (1985) extended to high salinity. Depth integrated samples were collected from the shallow lagoon at the sampling sites, and mat pore water and sediment pore water were extracted under pressure in the field using a series of 10 cm diameter cores in 1 cm depth increments. Alkalinity (as HCO<sub>3</sub><sup>-</sup>) was determined using inflection-point (Gran) titration with 0.01 M HCl (precision ±0.5%). All the samples for cation and anion analysis were filtered, stored at <4°C in high-density polyethylene (HDPE) bottles, and subsequently weight diluted for the analysis of major cations (Na<sup>+</sup>, Ca<sup>2+</sup>, Mg<sup>2+</sup> and K<sup>+</sup>) and anions (Cl<sup>-</sup> and SO<sub>4</sub><sup>2-</sup>), using inductively coupled plasma - optical emission spectrometry (ICP-OES) and UV/Vis spectrophotometry, respectively. Analyses gave a combined ion balance error of  $1.9 \pm 3.9\%$ . <sub>p</sub>CO<sub>2</sub> and saturation indices (logIAP/K) for carbonate and evaporite minerals were calculated with PHREEQC version 3 using the Pitzer equation for calculation of solute activity (Parkhurst & Appelo, 2013).

## **RESULTS**

## Hydrochemistry of the microbial mat

The hydrochemistry of the Mesaieed water overlying the mat, within the microbial mat itself, and the mud deposit underlying the mat, have been partially presented in Słowakiewicz *et al.* (2016); in this paper, the full dataset is presented, including new measurements from the

carbonate mud underlying the mat (Fig. 3). Surface waters above the mat sampled in summer 2013 and winter 2014 had salinities ca 64% and ca 41%, respectively (Słowakiewicz et al., 2016), the former being significantly elevated relative to samples of local nearshore seawater (40 to 49‰), reflecting the effect of summer evaporation in the restricted lagoon. Through the mat, in summer, with increasing depth from the surface there was a reduction in salinity from 61% at 1 cm to 46% at the base of the mat at 6 cm. Salinity in the top 10 cm of the underlying sediment was ca 41%. The shallow water overlying the mat was highly alkaline, with pH of ca 8.8 to 9.5 and 9.1 in summer and winter, respectively, compared to ca 8.2 for the local seawater. The water overlying the mat was also characterised by very high daytime dissolved O<sub>2</sub> (290% and 159 to 205% saturation; Fig. 3), the result of cyanobacterial photosynthetic activity at the surface of the mat and strong drawdown of CO<sub>2</sub> in the nearshore seawater (Fig. 3). Dissolved O<sub>2</sub> levels declined dramatically in the very shallowest part of the mat, to 3.6% at 1 cm depth and reached the limit of detection (0.1%) at the base of the mat and into the sediment below (Fig. 3). Thus, the system was anoxic beneath the surficial photosynthetic layer. The associated reduction in pH through the mat was more gradual, but by 2 cm pH had dropped below that of seawater, and reached 7.6 at the base of the mat. The  $_{p}CO_{2}$  of pore water increased rapidly with depth, reaching  $10^{\text{-}2.86}$  atm by the base of the mat, three orders of magnitude higher than the daytime PCO2 in the overlying lagoon water (Fig. 3). This might reflect the high CO<sub>2</sub> production by microbial metabolic reactions. The variation in PCO2 affects the saturation index (SI) with respect to the key carbonate minerals (Fig. 3). Surface water (daytime) above the mat was strongly supersaturated with respect to aragonite, calcite and dolomite, in excess of values for local seawater. The HCO<sub>3</sub> alkalinity exceeded that of seawater, confirming the role of photosynthesis rather than precipitation of carbonate minerals in controlling the drawdown of CO<sub>2</sub>. The maximum HCO<sub>3</sub> alkalinity was recorded in the upper 1 cm of the mat, with a value of 4 mmol, some 2.6 times that of the overlying lagoon water.

The maximum degree of supersaturation with respect to carbonate minerals occurred in the uppermost sample from the mat (0 to 1 cm), reflecting the particularly high alkalinity, despite the low dissolved O<sub>2</sub> content. Beneath this, carbonate mineral SI declined with depth and approached aragonite equilibrium in the sediment beneath the mat. The dolomite SI followed a similar trend, varying over two orders of magnitude, but all samples remained dolomite supersaturated. In contrast, all samples were undersaturated with respect to gypsum, the dominant local evaporite mineral (Whitaker *et al.*, 2014).

## Organic matter and minerals

## Authigenic minerals associated with organic matter

Authigenic minerals occur within the topmost layer of the mat and down through the whole mat thickness. These minerals are closely associated with all types of micro-organisms inhabiting the mat and commonly are enveloped by, or in continuity with, large amounts of EPS (Figs 4 and 5). Extracellular polymeric substances are widespread in the mat because they are produced by most of the bacterial forms (Fig. 4A and B). Cyanobacteria and chains of *Beggiatoa* cells are covered by a thick mucilaginous sheath several hundreds of microns long (Fig. 4C). Non-filamentous forms, isolated or in colonies, are also commonly immersed in abundant polysaccharide mucus (Fig. 4D).

Microscopically, EPS (which are just a few nanometres thick) are composed of a network of randomly scattered, polymeric threads organized to form a two-compartment structure with an inner layer, tightly and stably bound to the cell surface, and a loose and dispersed outer layer without an obvious and clear profile (Fig. 4D; see also Figs 8 to 10).

Authigenic minerals are observed nucleating within EPS (Fig. 5A and B). This process of mineralization commonly takes place within all the layers of the mat, and is particularly evident where bacterial cells themselves are also mineralized (Fig. 5C and D). In any case, during the investigation of the various layers of the mat, it was possible to observe that the mineralization (partial or complete) of the bacterial cells is much less common compared to EPS mineralization. In fact, integrating and comparing SEM and TEM observations of the early stages of the process of organic matter mineralization, shows that the initial sites of mineral nucleation and accretion are almost exclusively within the EPS that surround the bacterial cells, and in this initial stage the cells themselves are rarely mineralized (Fig. 6). Moreover, the interstitial fluid between the microorganisms lacks any neo-formed minerals (Fig. 6C and D).

The very early stages of EPS mineralization are clearly observed through the high magnification of the TEM, which shows the development of inorganic nanoparticles, a few tens of nanometres in size, along the threads that compose the EPS (electron-dense dark areas in Fig. 7A and B). Nanoparticles initially replicate the structure of the EPS and gradually aggregate to form larger masses, irregular to sub-spherical in shape (Fig. 7A to D). At this early stage of development, chemical analyses obtained with EDS with both SEM and TEM instruments show that nanoparticles are composed of Ca [36 to 58% (46)], Mg [7 to 19% (17)], Si [9 to 25% (18)], S [2 to 8% (4.5)], Al [4 to 7% (5.5)] and Fe [0 to 2% (1.3)] [range of moles % without O and C, and average (in brackets)], associated with a large amount of O

and C that can reach 60%. These particles are most probably amorphous, since their composition does not correspond with any known mineral; this is also implied by the absence of X-ray diffraction peaks (SAED) recorded during TEM observation.

Furthermore, elemental composition maps of mineralizing EPS confirm the development of nanoparticles, but also show an accumulation of Ca, Si, Al, S and Mg within the EPS as a whole, rather than just coinciding with the nanoparticles (Fig. 8). Carbon, oxygen and nitrogen are obviously present and account for at least 95 to 98% of the total element composition, as detected by selected area EDS analyses. It seems that this process of element accumulation does not substantially affect the ultra-structure of the EPS, as is evidenced by the preservation of the thread-like structure characterizing the mucus (Fig. 8B). This process predates the formation of the amorphous nanoparticles and suggests a preliminary role of the EPS as an attraction site for the elements. The nucleation sites for the successive formation of the amorphous nanoparticles seem to be located first in the peripheral areas of the EPS and then subsequently within the remaining zones.

As the dimension of the mineral precipitates increases they start to develop a sort of crystal habit or at least crystal terminations (Fig. 7A to D). In fact, true crystal units, i.e. solid units with a crystalline structure and a chemical composition referable to known minerals, even if largely <1 μm, are detectable in more mineralized EPS. Two types of nanocrystal can be distinguished; a fibrous and an ovoid/irregular form (Fig. 9A). The former consists of elongate fibrous crystals, *ca* 0.05 to 0.1 μm wide and 0.1 to 0.5 μm in length, whereas the latter consists of ovoids or irregular masses, 0.05 to 0.4 μm in diameter: SAED associated with TEM confirms the crystalline structure of such mineral units (Fig. 9B). The composition of these nanocrystals, analysed by EDS, is as follows; fibrous crystals are composed of Si (46 to 75%), Al (2.4 to 3.6%) and Mg (7 to 40%), with traces of Fe, Ca, Na and S (range of moles % excluding oxygen); the ovoidal to irregular crystals are composed of Ca (65 to 93%), Mg (2 to 31%) and low S (range of moles % excluding C and O). Considering the average composition and the habit of the two minerals, the fibrous crystals can be referred to a clay mineral, whereas the irregular masses are a Ca-carbonate mineral with a variable amount of Mg.

Descending into the mat, from the first millimetres down to 4 cm (Fig. 2), the amount of mineral matter increases with respect to the organic component (Fig. 10A). The carbonate and the clay form micron-sized masses that commonly aggregate to form clusters or peloids, of variable dimension between 10  $\mu$ m and 200  $\mu$ m (Fig. 10B). Peloids show irregular to subovoidal shapes. The two mineral phases are randomly distributed in the peloids with the clay

mineral providing a sort of matrix enveloping the carbonate (Fig. 10C to F). The mineral units forming the peloids that are generally a few microns in size, show a variable habit; in particular, carbonate minerals make the transition from anhedral to euhedral crystals, and also from smaller to larger dimensions (Fig. 10D and F). This transition seems to be related to the position of the mineral within the mat, as larger and better developed crystals occupy deeper layers within the mat. The fibrous clay crystals on the other hand do not show any particular variations.

There are peloids composed entirely of carbonate mineral matter (Fig. 11). In most of the cases measured the carbonate shows a composition rich in trace elements of the order of Mg 3.0%, Na 6.5%, S 2.2% and Sr 1.9% (moles %). The presence of a few moles of Sr could indicate the mineral aragonite. In a few cases, the composition suggests a very high-Mg calcite (VHMC) or Ca-rich dolomite (a few moles of Ca in excess of the stoichiometric ratio) with traces of S at *ca* 1.0%. The aragonitic carbonate peloids are particularly rich in mineralized bacterial cells and EPS (Fig. 11A and B). Some Ca-carbonate peloids are composed of a cluster of sub-ovoidal crystallites, a few microns in size, which result from the aggregation of sub-micron sized fibrous nanocrystals (Fig. 11C and D).

Finally, pyrite appears around a depth of 2 cm in the mat with cubic nanocrystals (<1  $\mu$ m). These commonly aggregate to form sub-spherical framboids 5 to 10  $\mu$ m in size (Fig. 12).

## Biogenic grains and minerals after organic matter removal

The SEM images of the finer particles from samples with the organic matter removed revealed few biogenic grains; fragments of diatoms, coccoliths and foraminifera were observed. The few diatoms are poorly preserved which could be the result of some dissolution within the mat. One coccolith has micron-sized, equant crystals on the surface which might be an early syntaxial cement. Of the mineral matter, only amorphous material was observed in a sample from the uppermost layer; no crystal forms or their incipient precursors were observed there.

X-ray diffraction of the residues from samples deeper within the mat detected several minerals (Fig. 13); aragonite (A), low-Mg calcite (LMC), high-Mg calcite (HMC), dolomite (and/or VHMC, because the ordering peaks of dolomite are very weak or absent) and quartz. Clay mineral peaks are also present, the most prominent of which are at  $8.4^{\circ}$  and  $27.7^{\circ}$  20 (CuK $\alpha$ ), i.e. characteristic for palygorskite.

The minerals present are calcite, crystallites commonly arranged into cones which then develop into crystals with terminations, aragonite and, less commonly, rhomb-shaped carbonate minerals with a high-Mg content (HMC, VHMC/dolomite). There are also fibres and felted sheets of clay mineral composition. Of particular interest is the presence of nanosized and micron-sized spheroidal structures, which are in the process of being permineralized.

## Calcite crystallite bundles and crystals

The most conspicuous precipitates within the mid to lower parts of the microbial mat (layers from 1 to 4 cm depth in Fig. 2) are elongate crystallites mostly forming cone-shaped bundles and crystals themselves (Figs 14 and 15). From EDS spot analyses, these are composed largely of Ca, values of 14.8 to 30.4% the rest C and O, and so they are a carbonate; they have a low-Mg content (0 to 0.9%), indicating a low-Mg calcite mineralogy. The crystallites and crystals occur together. The crystallites generally form cone-shaped bundles, from 0.5 to 20 μm in length, but mostly 3 to 5 μm (Fig. 14A and B). The individual crystallites increase in width upward in the conical bundles, and diverge away from the point of origin with an angle of around 20 to 30°. Crystallites are also precipitated higher up on the outer surface of a cone, usually in their own smaller bundle (or sub-bundle). Where the substrate of nucleation is visible, individual cones commonly have their own nucleation site, distanced from that of neighbours by a few micron (Fig. 14D). In one case, EDS analysis shows that a crystallite bundle is dominated by Ca (carbonate), but the substrate upon which it grew is a Ca-Mg carbonate (VHMC/dolomite; Fig. 14D). In other situations, several cones extend out from one nucleation point, to form a stellate pattern (Fig. 14C) or two have grown in opposite directions to form a dumb-bell (Fig. 14E).

In cross-section, the crystallite bundles vary from circular to triangular, from the presence of three crystal faces (Fig. 14B and F), to more hexagonal with six crystal faces present, of alternating wider and narrower faces (Fig. 15). The tops of the crystallite bundles, 0.5 to 1 µm across, vary in appearance from near-flat, where all crystallites are finishing at the same level, to a more 'ragged' collection of crystallites of different lengths, to a hemispherical – domal top (i.e. like that of a cone of ice cream (Fig. 14E). Other conical crystallite bundles have crystal terminations. In some cases, a gap or groove is present where the crystal faces of the termination are growing together; in other situations, this has disappeared and there is a sharp join between the faces (Fig. 15A to C). A hole is commonly present in the centre of the terminations where the three faces are going to meet at the apex

(Fig. 15C and D); this has a vague to distinct triangular shape. A complete trigonal crystal termination is present where the apical hole has been filled (Fig. 15D). The surfaces of crystal faces vary from rough, with a nanometre-scale topography, to a completely smooth surface where the crystal form is complete (Fig. 15E and F).

# Aragonite

This mineral was not as frequently encountered as calcite and is recognised by it needle to columnar crystal form (Fig. 16) and low-Mg content. These crystals are elongate, 2 to 4  $\mu$ m in length and <0.5  $\mu$ m in width, and tend to occur as clusters and aggregates.

#### *Very high-Mg calcite – dolomite*

Crystals with a high-Mg and Ca content from EDS, likely to be very high-Mg calcite (VHMC) or dolomite, were observed locally in the lower layers of the mat; they are roughly rhombic in shape (Fig. 16A and B) and have a size from 1 µm up to 20 µm. In one case a 'layering' to the crystal can be seen (Fig. 16B), and there are small fibres on the crystal surface, probably palygorskite (see below).

## Clay minerals

Fibres of clay minerals are very common in the Qatar microbial mat, especially in the lower layers. They are often seen as fragments of felted mats, several tens of microns across. The fibres themselves are commonly 5 to 10 µm in length, rarely up to 20 µm, and a few tens of nanometres across (Fig. 16C). Mostly they are straight but some are curved. The tips of the fibres in some cases are quite prominent, slightly larger than the width of the fibre itself (Fig. 16D). The fibres forming the mats have a variable density and roundish holes or gaps are present (Fig. 16E), with the fibres folded around. The fibres may be near-parallel and arranged into sheets or quite random in their occurrence in the mat. EDS shows that the dominant elements in the fibres are Mg and Si, with some showing small peaks of Al and Ca.

#### Spheroidal structures: nanospheres and microspheres

Spheroidal structures are common in the Qatar microbial mat and two types are distinguished based on size. These two types are nanospheres and microspheres.

#### **Nanospheres**

Nanospheres, some of which are permineralized, are clearly seen with both SEM and TEM. With the SEM, coccoidal bacterial cells, 1 to 2 µm in diameter, commonly show nanospherical bodies a few tens of nanometres to 100 nm in diameter, attached to the external wall of the cell (Fig. 17A). In some cases, a connecting 'stalk' can be distinguished between the nanosphere and the cell (Fig. 17B). The nanospheres are usually polyhedral in shape, rather than being truly spherical; in other words they appear to have straight edges and planar surfaces, suggesting the shape is icosahedral (Fig. 17B). There are commonly clusters or accumulations of nanospheres too, all of a similar size (30 to 60 nm), closely associated with EPS (Fig. 17). These form peloid-like structures 1 to 2 µm in diameter (Fig. 17C).

The SEM BSE images show that some of the nanospheres are permineralized rather than just being organic matter (Fig. 17C). The EDS reveals that the nanospheres consist of variable, but generally low amounts of Ca, Mg, S, Si, Al and Fe, but with higher contents of Ca in some cases; most abundant though are C and O.

With the TEM, bacterial cells from the microbial mat are clearly seen. Coccoid cyanobacteria are mostly 1 to 2 µm in length, circular to oval to elongate in the sliced section; they are readily distinguishable by the presence of thylakoid structures (the sites of photosynthesis in the prokaryotic cells), appearing as a collection of near-parallel lamellae or membranes, locally curved (Fig. 18A and C). Cells not containing this stripy material are probably sulphate-reducing bacteria. In some cases, there is an obvious coating of EPS around the bacteria, several 100 nm thick, with a dark, thread-like appearance (Fig. 18A and B).

Nanospheroids are frequently observed inside bacterial cells with the TEM (Fig. 18). In some cases, the cells do not appear to have a definite outer membrane, probably because this has disintegrated, and one sees a collection of nanospheres and the thylakoids (Fig. 18C). The TEM image is a cross-section so the nanospheres appear to have variable sizes, 30 to 150 nm. Many nanospheres have no internal features; there is just a thin dark outer margin to the particle, a few nanometres thick. Some do show small patches of dark matter within the spheroid; this could be an initial precipitate of amorphous material (Fig. 18B and C). Nanospheres are also observed dispersed in the areas surrounding the cells, which would have been fluid originally. These nanospheres may be composed of organic matter, but some show low concentrations of cations, through the presence of Ca, Mg, S, Si, Al and Fe in EDS analyses (for example, Fig. 18B and C). The degree of order of these mineral nanospheroids

is very low; in fact they are mostly composed of amorphous material since there is an absence of diffraction peaks from the TEM-SAED.

# **Microspheres**

There are numerous microspheroids present within the microbial mat from Qatar; these are generally from 1 to 10 µm in diameter, i.e. one or two orders of magnitude larger than the nanospheres. These vary from spheroidal to ellipsoidal in shape, with some having flat surfaces (Fig. 19A). The surfaces of the spheroids are mostly smooth although some are quite rough, appearing to be composed of finely crystalline particles (Fig. 19B). Some coalescence of these spheroids also appears to be taking place to form aggregates or more sheet-like material (Fig. 19C). The composition is variable; smooth ones tend to be a mixture of Ca, Mg, Si and Na, with high C and O; some are composed of Ca (± Mg) carbonate. Some finely crystalline ones (Fig. 19B) are dominated by Fe (16%), C (16%) and O (60%), with low Ca (4%), suggesting that it is an iron carbonate, like siderite–ankerite, although no Mg was recorded.

## **DISCUSSION**

# Amorphous nanoparticles and carbonate and clay mineral biomineralization

Calcium/Mg-carbonates and clay mineral fibres nucleate and grow within all the layers of the mat (Fig. 2), and the EPS are the main site of mineral nucleation for both mineral species. The process begins with the formation of nanoparticles, a few tens of nanometres in size, that replicate the EPS ultrastructure up to its complete permineralization. The resulting nanoparticles are amorphous (i.e. without crystal shape and crystalline structure) and show a composition that includes Ca, Mg, Si and Al, and less S and Fe. The nanospheroidal and microspheroidal structures also begin as organic-rich particles which gradually become permineralized.

Carbonate nanoparticles and nanospheres have commonly been recognized as initial elemental units resulting from microbial-mediated mineralization processes. Calcite consisting of an aggregation of mineral nanoparticles (non-classical crystallization of Niederberger & Cölfen, 2006) has been documented as a common biosignature of modern and ancient microbial carbonate (López-García *et al.*, 2005; Benzerara *et al.*, 2006, 2010; Perri & Tucker, 2007; Bontognali *et al.*, 2008; Sànchez-Romàn *et al.*, 2008; Manzo *et al.*, 2012; Perri & Spadafora, 2011; Perri *et al.*, 2012a,b; Bahniuk *et al.*, 2015). Dupraz *et al.* (2009) suggested that a local increase in alkalinity and supersaturation within microdomains

of the EPS induce the formation of an amorphous calcite gel, followed by the production of nanospheres from a mixture of amorphous calcite and acidic EPS macromolecules. Successively, nanospheres act as seeds for further carbonate crystallization. However, following Decho (2010), once nucleation has commenced, the calcium carbonate precipitate can develop as a growing crystal (i.e. a purely mineral form) or as an amorphous precipitate, or as a mixture of the two. Within the confines of the EPS matrix (and biofilms) the precipitate forms can exist along a continuum, ranging from individual highly-ordered crystals to disordered clusters of organic-rich amorphous precipitates. More recently nanospheres of amorphous calcium carbonate (ACC) have also been recognized in microbial-mediated ooids on the Great Bahama Bank (Diaz *et al.*, 2015) and microbial carbonate of Gongxiaoshe and Zhuyuan hot springs, China (Jones & Peng, 2014).

Nanoparticles observed in the Mesaieed mat do not have a pure Ca/Mg carbonate composition, because a conspicuous component of Si and Al is present. Moreover, this study observed that the same nanoparticles that act as seeds for carbonate crystallization represent a good substrate for successive clay mineral formation. The clay can replicate the EPS structure in a similar way to the carbonates and it is strictly associated with carbonates to form peloids. All of this implies the authigenesis of the clay mineral and biotic mediation in its formation.

As reported in Calvo *et al.* (1999), a variety of authigenic clay minerals commonly form in continental saline environments. In most cases, significant removal of Mg<sup>2+</sup>, enhanced by the reaction with silica from the lake waters, results in the formation of magnesium silicates. Magnesium-smectite (for example, stevensite), kerolite and sepiolite are rather common authigenic clay minerals, together with palygorskite, which is also present in many soils of arid to semi-arid regions. Mass-balance calculations carried out for saline lakes indicate that solute loss of K, Mg and Si contributes to the formation of the authigenic clay minerals, whether through transformation of pre-existing clays or by direct precipitation from the saline solution.

Bacterial mediation in the formation of clay minerals is not an unknown process. The most frequent observation of biogenic clay phases comes from biofilms in freshwater lakes and rivers where Fe/Al silicates are the most common (Konhauser, 1997, 2007). It is particularly remarkable that irrespective of the chemical composition of the water from which they form, microbial-mediated clays begin to form as nanoparticles (<100 nm) within the EPS surrounding the cells, with an amorphous or poorly-ordered ultrastructure. Biogenic clay minerals have also been observed in soils, freshwater microbial mats, and in deep sea deposits (Köhler *et al.*, 1994; Tazaki, 1997, 2006). Magnesium-iron silicates have been

reported in association with hot-spring carbonate deposits in the Ruidian geothermal area, China (Jones & Peng, 2014), and observed in deep sea sediments from Iheya Basin, Japan (Ueshima & Tazaki, 2001).

Authigenic poorly-crystallized magnesium silicates, for example stevensite, kerolite and sepiolite, are now known to be components of microbialites in modern saline and alkaline lakes: in the Lake of Satonda, Indonesia (Arp *et al.*, 2003; Benzerara *et al.*, 2010); in Lake Clifton, Australia (Burne *et al.*, 2014); in Lake Van, Turkey (Kempe *et al.*, 1991; López-García *et al.*, 2005; Benzerara *et al.*, 2006); in Mono Lake, California (Souza-Egipsy *et al.*, 2005); in basaltic caves, Hawaii (Léveillé *et al.*, 2000a,b, 2002, 2007), and finally in the lakes Quechulac, La Preciosa and Atexcac, Mexico (Zeyen *et al.*, 2015).

More recently Pace *et al.* (2016) observed a Mg-Si phase associated with carbonates in the lithifying microbial mat of Great Salt Lake (Utah) and proposed a biotic mechanism for the precipitation of the minerals, through three steps progressing along geochemical gradients produced through microbial activity: (i) a poorly-crystallized Mg-Si phase precipitates on an alveolar extracellular organic matrix due to a rise of the pH in the zone of active oxygenic photosynthesis; (ii) aragonite patches nucleate in close proximity to sulphate reduction hotspots, as a result of the degradation of cyanobacteria and extracellular organic matrix mediated by, among others, sulphate-reducing bacteria; and (iii) partial replacement of aragonite by dolomite, possibly in neutral to slightly acidic pore water. This might occur due to dissolution–precipitation reactions when the most recalcitrant part of the organic matrix is degraded.

Finally, an amorphous early mineral phase rich in Mg and Si has been observed in association with EPS in the coastal sabkha of Abu Dhabi (United Arab Emirates), and it has been interpreted as a precursor phase evolving to dolomite (Bontognali *et al.*, 2010). Here, the authors showed that mineral precipitation is initiated within the EPS that appears as an alveolar organic network, which is progressively replaced by mineral precipitation consisting firstly of an amorphous precipitate that forms on the walls of the EPS alveolar structure rich in Mg and Si.

As has been described above, within this microbial mat from Qatar, a range of minerals is being precipitated, with the early amorphous material forming in the top layer of the mat clearly linked to the EPS-bacterial organic matter there. The subsequent development of better-defined crystals, of carbonate or silicate, is probably an inorganic process, once they have been initiated on nuclei within the amorphous material or the latter has recrystallized into nanometre-sized crystallites through some maturation-crystal growth mechanism. The

actual mineralogy of the crystals precipitated within the mat will be determined by cations adsorbed on to the EPS, pore water composition, pH-alkalinity and redox. The early formation of the amorphous Ca–Mg–Si material in the top layer is likely a reflection of the availability of Ca–Mg–Si in seawater and the supply of further ions from dissolution of wind-blown dust and biogenic grains (calcareous bioclasts, clay and diatoms) in that top millimetre of the mat where the pH and redox state change significantly from the lagoon-seawater above (Fig. 3). In this mat, Mg is taken out with the Si to form the abundant palygorskite. This could account for the dominant carbonate crystals being calcite (low-Mg) with subordinate aragonite and dolomite.

#### Role of extracellular polymeric substances before nanoparticle formation

Elemental composition maps of mineralizing EPS show the development of amorphous nanoparticles as the initial stage of mineral formation. Moreover, maps also show the accumulation of Ca, Si, Al, S and Mg within the whole EPS (Fig. 8), without affecting the thread-like ultra-structure of the EPS (Fig. 8B). This process predates the formation of the amorphous nanoparticles and suggests a preliminary behaviour of the EPS to the formation of the minerals there, firstly in the peripheral areas and successively within the whole EPS, and an accumulation of the ions necessary for successive nanoparticle and mineral growth.

The physicochemical properties of the polymer matrix, such as acidity or functional group composition, are important factors in the metal binding potential and biotic and abiotic degradation or alteration of the EPS favouring calcium carbonate precipitation (Dupraz & Visscher, 2005). The highly hydrated nature of much EPS represents an environment where ions and/or molecules can accumulate to reach higher concentrations (compared to the ambient fluid phase) (Decho, 2012), especially when they are produced or released more rapidly than diffusion or other forms of mass transfer can remove them (Sutherland, 2001). Such localized accumulations of ions, such as O<sub>2</sub>, Ca<sup>2+</sup> and H<sup>+</sup>, have been measured within the EPS matrices of microbial mats (Visscher et al., 1998; Braissant et al., 2009; Decho et al., 2009). In particular, Braissant et al. (2009) analysed high-Mg calcite-lithifying and nonlithifying EPS within a hypersaline microbial mat on the bottom of a very shallow lake (Eleuthera, Bahamas). The authors found that both EPS layers showed a very similar elemental composition: C, O and N, with S and Ca around 2% of the total. Microbial degradation of EPS produces HCO<sub>3</sub>, increases the alkalinity, and reduces the quantity of cation-binding sites, releasing cations such as Ca<sup>2+</sup> and Mg<sup>2+</sup>. Furthermore, microbial and/or abiotic degradation of EPS provides the necessary nucleation sites for mineral precipitation.

Another factor in microbial carbonate precipitation could be the presence of polysaccharides in the pore fluids, derived from micro-organisms and EPS. These appear to reduce the energy barrier to desolvation of Mg-ions, promoting the incorporation of Mg into precipitating carbonate, leading to disordered dolomite formation (Zhang *et al.*, 2012a,b).

In the case of freshwater biomediated clay minerals, Fe and ferric hydroxide are the most common ions adsorbed by the EPS. These allow the formation of amorphous (Fe, Al)-silicate phases binding dissolved silica, aluminium or aluminosilicate complexes (Konhauser & Urrutia, 1999; Davis *et al.*, 2002). Ueshima & Tazaki (2001) proposed that the formation of nontronite in deep sea sediments is induced by the accumulation of Si and Fe ions from the ambient seawater in the EPS, and that EPS serve as a template for layer-silicate synthesis. If acting as an 'ionic binder' EPS molecules seem particularly favourable for ion accumulation because of their high surface area; bacterial cells composed of peptidoglycan can act as nucleation sites for mineralization (Ferris *et al.*, 1986; Urrutia & Beveridge, 1993, 1994, 1995). Moreover, Urrutia & Beveridge (1993) suggested a cation bridging mechanism in which multivalent metal cations complex with an organic fabric (for example, COO<sup>-</sup>) that in turn bridges with ionic silicates to form large aggregates.

The role of EPS in accumulating cations that predate the formation of carbonates or clay minerals is then well-known; what is shown in this study for the first time, is the accumulation in bacterial EPS of a marine hypersaline mat, of a mix of Ca, Si, Al, S and Mg with various proportions, that could have played a fundamental role in the subsequent formation of both carbonate and clay minerals.

## Calcite crystallite bundles and crystals

The clear trigonal form of the conical crystallite bundles once they have developed into crystal structures indicates that their composition is likely to be calcite, rather than aragonite (or dolomite). The EDS analyses with dominant Ca and much lower to little or no Mg support a calcite mineralogy with a moderate to low-Mg content. There is no suggestion that these crystals are a very high magnesian calcite (VHMC). The rhombohedral-type terminations on the crystals are similar to the familiar nail-head calcite spar crystals, rather than the more elongate scalenohedral (dog-tooth) crystals. The growth of calcite crystals from a cone of diverging needle-like crystallites through to an organised trigonal-hexagonal prismatic crystal form, which develops into a crystal with a rhombohedral termination, is well-recorded by the SEM images presented here, and that is shown schematically in Fig. 20. Upward increasing width of crystallites and bundles/sub-bundles could well be the result of split-crystal growth.

Where growing on a flattish substrate (at the micron-scale), like a silt-sized bioclast fragment, then it is noteworthy that the crystal bundles are quite regularly spaced, and growing vertically, to give separate cones, with the space between them gradually being reduced upwards as the bundles grow and expand outward. Interference between bundles is not seen in these arrangements. Similar crystallite bundles have been described by Sánchez-Navas *et al.* (2013) and dumb-bell-type features illustrated by Warthmann *et al.* (2005).

Clearly important here is the rate of nucleation of crystallite bundles and the presence of dispersed nucleation points. Since the majority of crystallite bundles have a nanometre point of initiation, it is possible that they all form from a nucleation point which itself may have been of nanometre size, rather than developing 'free-floating' within the microbial mat. The extremely tiny point of initiation of the crystallite bundles is still present even when the crystals are >10 µm in length with crystal terminations. It is possible that in some cases the initial seeds for calcite crystallite growth were provided by the amorphous calcium carbonate (ACC) precipitated within the upper layer of the mat, or the nanospheres, described above and interpreted below. The upward expanding growth of the crystallite bundles through time is likely to have been through growth of sub-bundles of crystallites on the sides of earlier precipitates, with crystallographic control exerted by the earlier crystallites on the later ones. With further development, the conical–trigonal structures do come together and interfere, so that eventually certain crystals in a favoured orientation with faster growth (in the c-axis direction) take over in a form of competitive growth.

## Very high-Mg calcite/dolomite

In the case of the micron-sized rhombic crystals (Fig. 16A and B) the question is whether they are precipitated within the mat or whether they are detrital. The well-formed crystal shape of some of the rhombs is likely to indicate growth within the mat. Dolomite is a major component of the exposed bedrock in Qatar. The Eocene Damm Formation is dominated by dolomite although that is very well-ordered and stoichiometric with all ordering peaks well shown on XRD. Precipitation of dolomite (perhaps via an amorphous VHMC) in the Qatar mat would be expected in view of the positive value of the dolomite saturation index (Fig. 3B). Dolomite has recently been recorded in microbial mats on the west side of Qatar at Dohat Faishakh (Brauchli *et al.*, 2016; Al Disi *et al.*, 2017), although this area was one of those sites in the Arabian Gulf from which dolomite was described back in the 1960s (Illing *et al.*, 1965).

## Clay minerals

The fibrous appearance of the clay minerals is typical of palygorskite and the EDS analysis would be consistent with this composition (MgAl)<sub>2</sub>Si<sub>4</sub>O<sub>10</sub>(OH).4(H<sub>2</sub>O). The arrangement of the fibres as mats is reminiscent of the appearance of EPS within microbial mats such that it is tempting to interpret the palygorskite as having been precipitated within sheets of EPS occurring around and between the microbial layers. The holes within the felted sheets of clay fibres are reminiscent of the alveolar holes reported within EPS (e.g. Dupraz *et al.*, 2004). Almost identical palygorskite clay sheets after EPS have been described by Mettraux *et al.* (2014) from Neoproterozoic microbialites in Oman, where precipitation within the EPS itself was hypothesized.

Wind-blown dust is likely to be a major source of fine particles as well as a source of cations from their dissolution in the near neutral-mildly alkaline pore-waters of the microbial mat. Engelbrecht *et al.* (2009) presented dust data from many Middle Eastern countries and for Qatar 65% of the particles (by mass) are between 2.5 μm and 10.0 μm in diameter, with 14% 1.0 to 2.5 μm, and 1% less than 1 μm. The average composition is *ca* 37% SiO<sub>2</sub>, 12% Al<sub>2</sub>O<sub>5</sub>, 5% MgO and 40% CaO. Precipitation of Mg-silicate within the Qatar mat is likely to have occurred considering the change in pH from highly alkaline in the lagoon water to only mildly alkaline towards to bottom of the mat (cf. Chagas *et al.*, 2016).

#### **Spheroidal structures**

Spheroidal structures have been described for many years now from microbial mats (e.g. Vasconcelos *et al.*, 1995; Dupraz *et al.*, 2004; Warthmann *et al.*, 2005; Sánchez-Román *et al.*, 2009; Bontognalli *et al.*, 2010; Bahniuk *et al.*, 2015) and their sizes are in the same range as those described in this study; tens of nanometres to microns. In some studies of mats and laboratory experiments involving bacteria and cultures (Sánchez-Román *et al.*, 2011; Krause *et al.* 2012; Zhang *et al.*, 2012a,b; Rodriguez-Blanco *et al.*, 2015), these spheroids are composed of dolomite or a very high Ca-Mg carbonate (VHMC) interpreted as a precursor to dolomite (see discussion of mineralogy in Gregg *et al.*, 2015). The occurrence of VHMC/dolomite in microbial mats, ranging from spheroidal structures to more crystalline rhombic forms, has led to the suggestion that this is microbial dolomite (see discussion in Kaczmarek *et al.*, 2017).

## **Nanospheres**

The nanospheres in the microbial mat described here are interpreted as viral-like particles, that is the viruses themselves or the capsids after the viral material has been injected into a host cell. A virus has an outer shell (called a capsid) composed of protein and within this is the viral material of DNA and RNA. Viruses are not truly living organisms like bacteria and people; they do not reproduce between themselves; instead they inject their viral material into host cells where numerous new viruses are then produced. Eventually, the host cell dies and the viruses burst out (a process referred to as lysis), ready to infect other bacterial cells. The empty capsid is abandoned and floats off, along with fragments of the bacterial cell. Viruses take many forms but in the marine realm they are roughly spheroidal in shape, although some have a tail through which the viral material is injected into the host cell. The common form of many viruses is icosahedral, i.e. a spheroid with flat sides, as is seen in the nanospheres of the Qatar mat. The nanospheres are also in the correct size range (30 to 300 nm) for viruses; their close association with bacterial, especially coccoid (prokaryotic) cells is also characteristic (Pacton et al., 2015). The SEM observation of nanospheres upon the external wall of bacterial cells (Fig. 17A and C) has caught the viruses in the act of infection, and their presence within the cells seen with the TEM records the growth of new viruses.

One other possible biological interpretation of the nanospheroids is that they could be mineralized bacterial vesicles. Bacteria produce huge numbers of vesicles which are tens to 100 nm in size, similar in appearance to viral particles except that they tend to be more truly spheroidal–ellipsoidal, rather than icosahedral (Biller et al., 2014). Vesicles do not have any internal structure, just a marginal dark membrane. Vesicles are mostly produced by or close to the bacterial cell wall, and they are then located around the outside of the bacteria; they are not attached to the bacteria. The purpose of vesicles has been a matter of debate but they are thought to act as a decoy to prevent an attack by viruses (Biller et al., 2014); they could also be a mechanism for the bacteria to store nutrients, notably N and P. Although some of the nanospheroids in the Qatar mat could be vesicles, the majority show the icosahedral shape and they occur within the whole volume of a bacterial cell, rather than concentrated around the margin. Hence it is suggested that a viral origin is the most probable for these nanospheroidal objects. For the nanospheres within the bacterial cells, one other possible origin is carboxysomes, organelles involved with carbon fixation (Yeats et al., 2008). However, although they are of a similar size and shape to viruses, they are usually opaque. Finally, as suggested previously by many authors (noted above, reviewed in Dupraz et al., 2009), some nanospheroids—nanoparticles could have been precipitated abiotically, in the presence of organic matter—EPS but not directly by micro-organisms.

The composition of the permineralized nanospheres is very similar to the initial Ca–Mg–Si–C–O amorphous material being precipitated within EPS in the mat, discussed earlier. In the same manner as EPS, it is likely that viral material also has a negative charge (Daughney *et al.*, 2004; Kyle *et al.*, 2008b) such that cations are attracted to initiate the permineralization process.

The potential role of viruses in near-surface geological processes has not been explored in any detail; indeed, the very presence of viruses in geological materials has only recently been appreciated. The association of likely viral particles with mineral precipitation is clearly shown in the examples presented here and has also been documented by Pacton et al. (2014) from microbial mats in a hypersaline lagoon in Brazil; in lacustrine carbonates from Central Asia (Pacton et al., 2015); and by De Wit et al. (2015) from a salt lake in northwest Spain where viruses are closely associated with Ca-Mg carbonates. The ability of viruses and EPS to attract cations through their negative charge is a key feature in the precipitation of crystallites containing alkali-metal (Ca, Mg, Ba and Sr) and other elements. The precipitation of carbonates in this manner may well be connected to the photosynthetic activities of cyanobacteria and algae, removing CO<sub>2</sub> from pore-fluids and generating HCO<sub>3</sub> ions, as suggested by many authors (see Dupraz et al., 2009). Dupraz et al. (2009) have also described nanospheres within EPS in a microbial mat that are a mixture of amorphous calcite and acidic EPS molecules; these were interpreted as being abiotic, the consequence of a local increase in alkalinity and supersaturation within microdomains of the EPS. The arrangement of the nanospheres described here, attached to the outer wall of coccoid bacteria (Fig. 17A and B), is consistent with a microbiological, viral origin, rather than a more abiotic process. Viruses can also be expected to be present within the EPS around and between the bacteria of a microbial mat, as they search out a suitable new host cell. Successively, nanospheres act as seeds for further carbonate crystallization. However, following Decho (2010), once nucleation has commenced, the calcium carbonate precipitate can develop as a growing crystal (i.e. a purely mineral form) or as an amorphous precipitate, or as a mixture of the two.

Once partially to completely permineralized viral material could well provide heterogenous nucleation sites for further mineral precipitation. This is particularly significant for the later precipitation of dolomite where the existence of nano-size VHMC-dolomite crystallites from virus permineralization could be the catalyst to permit more ordered dolomite to form. In hot springs, silicified viral particles have been described by Laidler &

Stedman (2010), Peng *et al.* (2013) and Jones & Peng (2014); experimental silicification of viruses has been achieved by Orange *et al.* (2011). In terms of size, size-range and shape, the silicified nanospheres are very similar to those illustrated here from Qatar. Viruses have also been invoked as an agent in the precipitation of iron minerals (Kyle *et al.*, 2008b) and this has been shown experimentally by Daughney *et al.* (2004).

# Microspheres

Some of the larger microspheroids are interpreted to be the result of intracellular permineralization within bacteria or the permineralization of the bacteria themselves. Others could be the result of further growth and aggregation of viral material (nanospheres) or simply inorganic precipitates. The precipitation of minerals within bacteria has been documented for over a century, notably the presence of calcite within the large bacterium Achromatium (see Gray, 2006), and sulphur granules within Beggiatoa. In recent years, further cases of intracellular precipitation have been documented including amorphous Ca-Mg-Sr-Ba carbonate spheroids in cyanobacteria within a biofilm in the highly alkaline Lake Alchichica, Mexico (Couradeau et al., 2012; Benzerara et al., 2014; Li et al., 2016). Similar Ca-Ba carbonate spheroids (with some Sr), also referred to as 'micropearls', are forming within unicellular eukaryotic phytoplankton within the waters of Lake Geneva (Jacquet et al., 2013; Martignier et al., 2017). Different organisms appear to produce spheroids of different composition (Ca-rich, Ba-rich and Sr-rich), apparently somehow pre-concentrating particular elements which are in low abundance in the ambient water itself. The dimensions and shapes of the microspheroids in the Qatar mat are similar to the spheroids observed by these authors. Although the composition of those within the Mesaieed mat appears to be that of an amorphous compound, it is likely that this would eventually evolve into a carbonate mineral. The reasons why these bacteria and algae produce intracellular mineral precipitates are unknown, but it is clearly an intracellular biologically-controlled process (Benzerara et al., 2014; Cam et al., 2015; Martignier et al., 2017).

#### **Peloids**

On a large scale, the carbonate and clay minerals in the Mesaieed microbial mat form irregular to sub-ovoidal shaped peloids, of variable dimension between 10  $\mu$ m and 200  $\mu$ m (Fig. 10B). The two mineral phases can be randomly associated in the peloids and; apart from the majority of peloids composed of the two mineral phases, peloids composed only of carbonate also exist. Peloids are surrounded by organic matter in the form of living micro-

organisms with EPS, through a transition zone in which the organic component is gradually substituted by the mineral part. This confirms the same process observed at the microscale and nanoscale.

Excluding the purely descriptive term 'peloid', referring to micritic aggregates of uncertain origin (McKee & Gutschick, 1969; Macintyre, 1985; Flügel, 2004), in the literature peloids have often been regarded as being autochthonous and benthic microbial in origin, because they constitute the most common microfabric of modern and ancient microbialites (Gebelein, 1974; Bertrand-Sarfati, 1976; Monty, 1976; Kennard & James, 1986; Dupraz & Strasser, 1999; Riding, 2000, 2002a). The most common peloidal microfabric consists of micritic peloids surrounded by microspar. However, it has been demonstrated that very similar micromorphologies can be created by purely abiotic mechanisms (Bosak *et al.*, 2004). Chafetz (1986) and Riding (2002b) suggested that peloids could be calcified aggregates resembling bacterial microcolonies in Phanerozoic fossil biofilms. Following studies on modern microbial mat lithification, the formation of peloidal carbonate precipitates has been associated with the metabolic activities of bacteria (Paerl *et al.*, 2001; Dupraz *et al.*, 2004; Riding & Tomás, 2006; Spadafora *et al.*, 2010; Perri *et al.*, 2012a).

The observations reported here on the Mesaieed mat confirm that the peloidal microfabric formed *in situ* during the very early stages of mineralization, due to the degradation and permineralization of organic matter (mainly EPS but also micro-organisms). Inter-peloid spaces can be filled successively by abiotic precipitation of microsparite, as the residual organic matter is removed (Spadafora *et al.*, 2010).

#### **CONCLUSIONS**

In the modern high-intertidal—lagoonal microbial mats of Mesaieed sabkha (Qatar) several autochthonous minerals are precipitated; calcite and palygorskite (Mg-rich clay) are the most common, whereas dolomite, aragonite, ankerite and pyrite are subordinate to rare. The initial precipitates within the top millimetres of the mat are composed of Ca—Mg—Si—Al—S amorphous nanoparticles (few tens of nanometres) that replace the ultrastructure of extracellular polymeric substances (EPS). The EPS are extensively enriched in the same cations and in this way they act as a substrate for mineral nucleation. Successively Mg—Si nanocrystals take the form of fibres of palygorskite associated with Ca-carbonate nanocrystals. This implies the biomediated origin of all these minerals with a mechanism of EPS replacement due to the degradation (biotic and/or abiotic) of the EPS itself.

When further analysing the developing carbonates it was observed that crystals of low-Mg calcite and aragonite are the most common precipitates together with fewer very-high-Mg calcite/dolomite and ankerite particles. Pyrite nanocrystals and framboids are present in the deeper layers of the mat.

Calcite crystallites grow from a nano-point of nucleation to form conical bundles. Growth in two or more directions leads to dumb-bell and stellate forms. The cones develop from circular to triangular to hexagonal in cross-section, and eventually terminations form to give rhombohedral (nail head) calcite crystals, 5 to 30 µm in length.

The source of silica for the Mg-silicates could be wind-blown dust or diatoms, with the Mg and Ca from seawater. Silica dissolution–Mg silicate precipitation, and carbonate precipitation, are likely to have been driven by pH–SI–redox changes within the mat, related to micro-environmental–chemical changes induced by the microbes–EPS and their degradation.

Nanospheroids and microspheroids are common in the microbial mat, varying in their degree of permineralization. The nanospheroids have the same size and shape as viruses, and they been observed attached to and within coccoid bacteria, exactly as reported for viruses. These nanospheroids are interpreted as virus-like particles and they could play a major role in carbonate precipitation by providing the nuclei to initiate the process, leading to the formation of crystallites and then in time to crystals. Microspheres are likely to be permineralized bacteria and intracellular precipitates, although with both nanospheroids and microspheroids some could be the result of simple abiotic precipitation. Finally, carbonates and clay minerals are commonly aggregated to form peloids, tens of microns in size, surrounded by residual organic matter, confirming that the peloidal fabric is also a biomediated texture.

#### **ACKNOWLEDGEMENTS**

We thank the Mesaieed Port Authority for permission to collect mats and J. Jameson and C. Strohmenger (Exxon Mobil Qatar Centre for Coastal Research) for introducing us to the area. We are indebted to S. Mey Didi-Ooi, G. Tong and J. Simmonds for field assistance and collection of some data. We also thank Hazel Sparkes at Bristol for XRD analyses and Jay Gregg for a detailed XRD analysis at the University of Oklahoma. MET is grateful to Alex Anesio, Professor of Biogeochemistry at Bristol, for discussions and banter. We gratefully acknowledge the critical and constructive comments of Giovanna Della Porta, Stephen Lokier and Robert Burne.

#### **REFERENCES**

Al Disi, Z.A., Jaoua, S., Bontognali, T.R.R., Attia, E.S.M., Al-Kuwari, H.A.A. and Zouari, N. (2017) Evidence of a role for aerobic bacteria in high magnesium carbonate formation in the evaporitic environment of Dohat Faishakh Sabkha in Qatar. *Frontiers in Environmental Science*, 5, 1.

Al-Thani, R., Al-Najjar, M.A.A., Al-Raei, A.M., Ferdelman, T., Thang, N.M., Al Shaikh, I., Al-Ansi, M. and de Beer, D. (2014) Community structure and activity of a highly dynamic and nutrient-limited hypersaline microbial mat in Um Alhool Sabkha, Qatar. *PLoS ONE*, **9**, e92405.

Allison, D.G., Gilbert, P., Lappin-Scott, H.M. and Wilson, M. (2000) Community structure and co-operation in biofilms. Cambridge, University Press, 349 p.

**Arp, G., Reimer, A.** and **Reitner, J.** (2003) Microbialite formation in seawater of increased alkalinity, Satonda Crater Lake, Indonesia. *Journal of Sedimentary Research*, **73**, 105–127.

Bahniuk, A., McKenzie, J.A., Perri, E., Bontognali, T.R.R., Vogeli, N., Rezende, C.E., Rangel, T.P. and Vasconcelos, C. (2015) Characterization of environmental conditions during microbial Mg-carbonate precipitation and early diagenetic dolomite crust formation: Brejo do Espinho, Rio de Janeiro, Brazil. *Geological Society, London, Special Publications*, 418, 243-259.

Benzerara, K., Menguy, N., López-García, P., Yoon, T.H., Kaźmierczak, J., Tyliszczak, T., Guyot, F. and Brown, Jr., G.E. (2006) Nanoscale detection of organic signatures in carbonate microbialites. *PNAS*, **103**, 9440-9445.

Benzerara, K., Meibom, A., Gautier, Q., Kaźmierczak, J., Stolarski, J., Menguy, N. and Brown, Jr., G.E. (2010) Nanotextures of aragonite in stromatolites from the quasi-marine Satonda crater lake, Indonesia. *Geological Society, London, Special Publications*, **336**, 211-224.

Benzerara, K., Skouri-Panet, F., Li, J., Férard, C., Gugger, M., Laurent, T. and Moreira, D. (2014) Intracellular Ca-carbonate biomineralization is widespread in cyanobacteria. *PNAS*, **111**, 10933–10938.

**Bertrand-Sarfati, J.** (1976) An attempt to classify Late Precambrian microstructures. In: *Stromatolites* (Ed. Walter, M.R.), Elsevier, Amsterdam, 251-259.

Biller, S.J., Schubotz, F., Roggensack, S.E., Thompson, A.W., Summons, R.E. and Chisholm, S.W. (2014) Bacterial vesicles in marine ecosystems. *Science*, **343**, 183-186.

**Bontognali, T.R.R., Vasconcelos, C., Warthmann, R.J., Dupraz, C., Bernasconi, S.** and **McKenzie, J.A.** (2008) Microbes produce nanobacteria-like structures, avoiding cell entombment. *Geology*, **36**, 663–666.

- Bontognali, T.R.R., Vasconcelos, C., Warthmann, R.J., Bernasconi, S.M., Dupraz, C., Strohmenger, C.J. and McKenzie, J.A. (2010) Dolomite formation within microbial mats in the coastal sabkha of Abu Dhabi (United Arab Emirates). *Sedimentology*, **57**, 824–844.
- **Bontognali, T.R.R., McKenzie, J.A., Warthmann, R.J.** and **Vasconcelos, C.** (2014) Microbially influenced formation of Mg-calcite and Ca-dolomite in the presence of exopolymeric substances produced by sulphate-reducing bacteria. *Terra Nova*, **26**, 72-77.
- Bosak, T., Souza-Egipsy, V., Corsetti, F.A. and Newman, D.K. (2004) Micrometer-scale porosity as a biosignature in carbonate crusts. *Geology*, **32**, 781-784.
- Braissant, O., Decho, A.W., Dupraz, C., Glunk, C., Przekop, K.M. and Visscher, P.T. (2007) Exopolymeric substances of sulfate-reducing bacteria: interactions with calcium at alkaline pH and implications for formation of carbonate minerals. *Geobiology*, **5**, 401-411.
- **Braissant, O., Decho, A.W., Przekop, K.M., Gallagher, K.L., Glunk, C., Dupraz, C.** and **Visscher, P.T.** (2009) Characteristics and turnover of exopolymeric substance in a hypersaline microbial mat. *FEMS Microbiology Ecology*, **67**, 293–307.
- Brauchli, M., McKenzie, J.A., Strohmenger, C.J., Sadooni, F., Vasconcelos, C. and Bontognali, T.R.R. (2016) The importance of microbial mats for dolomite formation in the Dohat Faishakh sabkha, Qatar. *Carbonates and Evaporites*, 31, 339-345.
- **Burne**, **R.V.** and **Moore**, **L.S.** (1987) Microbialites: organosedimentary deposits of benthic microbial communities. *Palaios*, **2**, 241-254.
- Burne, R.V., Moore, L.S., Christy, A.G., Troitzsch, U., King, P.L., Carnerup, A.M. and Hamilton, P.J. (2014) Stevensite in the modern thrombolites of Lake Clifton, Western Australia: a missing link in microbialite mineralization? *Geology* **42**, 575–578
- Calvo, J.P., Blanc-Valleron, M.M., Rodriguez-Arandia, J.P., Rouchy, J.M. and Sanz, M.E. (1999) Authigenic clay minerals in continental evaporitic environments. *IAS Special Publications*, **27**, 129-151.
- Cam, N., Georgelin, T., Jaber, M., Lambert, J.-F. and Benzerara, K. (2015) *In vitro* synthesis of amorphous Mg-, Ca-, Sr-and Ba-carbonates: what do we learn about intracellular calcification by cyanobacteria? *Geochimica et Cosmochimica Acta*, **161**, 36–49.
- **Canfield, D.E.** and **Des Marais, D.J.** (1993) Biogeochemical cycles of carbon, sulfur, and free oxygen in a microbial mat. *Geochimica et Cosmochimica Acta*, **57**, 3971-3984.
- Carreira, C., Staal, M., Middelboe, M. and Brussaard, C.P.D. (2015) Counting viruses and bacteria in photosynthetic microbial mats. *Applied and Environmental Microbiology*, **81**, 2149-2155.
- **Chafetz, H.S.** (1986) Marine peloids: a product of bacterially induced precipitation of calcite. *Journal of Sedimentary Petrology*, **56**, 812-817.
- **Chagas, A.A., Webb, G.E., Burne, R.V.** and **Southam, G.** (2016) Modern lacustrine microbialites: towards a synthesis of aqueous and carbonate geochemistry and mineralogy. *Earth-Science Reviews*, **162**, 338-363.
- **Characklis, W.G.** and **Wilderer, P.A.** (1989) Structure and function of biofilms. Dahlem Workshop Reports. *Life Sciences Research Report*, **46**, 386 pp.
- Couradeau, E., Benzerara, K., Gérard, E., Moreira, D., Bernard, S., Brown, Jr., G.E. and López-García, P. (2012) An early-branching microbialite cyanobacterium forms intracellular carbonates. *Science*, **336**, 459–462.
- **Daughney, C.J., Châtellier, X., Chan, A., Kenward, P., Fortin, D., Suttle, C.A.** and **Fowle, D.A.** (2004) Adsorption and precipitation of iron from seawater on a marine bacteriophage (PWH3A-P1). *Marine Chemistry*, **91**, 101–115.
- **Davis, C.H., Mathias, L.J., Gilman, J.W., Schiraldi, D.A., Shields, R., Trulove, P., Sutto, T.** and **De Long, H.** (2002) Effects of melt processing conditions on the quality of poly(ethylene terephthalate) montmorillonite clay nanocomposites. *Journal of Polymer Science: Part B: Polymer Physics*, **40**, 2661–2666.

- **De Wit, R., Gautret, P., Bettarel, Y., Roques, C., Marlière, C., Ramonda, M., Thanh, T.N., Quang, H.T.** and **Bouvier, T.** (2015) Viruses occur incorporated in biogenic high-Mg calcite from hypersaline microbial mats. *PLoS ONE*, **10**, e0130552.
- **Decho, A.W.** (1990) Microbial exopolymer secretions in ocean environments: their role(s) in food webs and marine processes. *Oceanography Marine Biology Annual Review*, **28**, 73-154.
- **Decho, A.W., Visscher, P.T.** and **Reid, R.P.** (2005) Production and cycling of natural microbial exopolymers (EPS) within a marine stromatolite. *Palaeogeography, Palaeoclimatology, Palaeoecology,* **219**, 71-86.
- **Decho, A.W., Visscher, P.T., Ferry, J., Kawaguchi, T., He, L., Przekop, K.M., Norman, R.S.** and **Reid, R.P.** (2009) Autoinducers extracted from microbial mats reveal a surprising diversity of N-acylhomoserine lactones (AHL's) and abundance changes that may relate to diel pH. *Environmental Microbiology*, **11**, 409–420.
- **Decho, A.W.** (2010) Overview of biopolymer-induced mineralization: what goes on in biofilms? *Ecological Engineering*, **36**, 137-144.
- **Decho, A.W.** (2012) Chemical communication within microbial biofilms: chemotaxis and quorum sensing in bacterial cells. In: *Microbial Extracellular Polymeric Substances*. *Characterization, Structure and Function* (Eds J. Wingender, T.R. Neu and H.-C. Flemming), pp. 155-169. Springer-Verlag, Berlin, Heidelberg.
- Diaz, M.R., Swart, P.K., Eberli, G.P., Oehlert, A.M., Devlin, Q., Saeid, A. and Altabet, M.A. (2015) Geochemical evidence of microbial activity within ooids. *Sedimentology*, **62**, 2090-2112.
- **Dupraz, C.** and **Strasser, A.** (1999) Microbialites and micro-encrusters in shallow coral bioherms (Middle–Late Oxfordian, Swiss Jura Mountains). *Facies*, **40**, 101–130.
- **Dupraz, C., Visscher, P.T., Baumgartner, L.K.** and **Reid, R.P.** (2004) Microbe-mineral interactions: early carbonate precipitation in a hypersaline lake (Eleuthera Island, Bahamas). *Sedimentology*, **51**, 745-765.
- **Dupraz, C.** and **Visscher, P.T.** (2005) Microbial lithification in marine stromatolites and hypersaline mats. *Trends in Microbiology*, **13**, 429-438.
- **Dupraz, C., Reid, R.P., Braissant, O., Decho, A.W., Norman, R.S.** and **Visscher, P.T.** (2009) Processes of carbonate precipitation in modern microbial mats. *Earth-Science Reviews*, **96**, 141-162.
- Engelbrecht, J.P., McDonald, E.V., Gillies, J.A., Jayanty, R.K.M., Casuccio, G. and Gertler, A.W. (2009) Characterizing mineral dusts and other aerosols from the Middle East Part 2: grab samples and re-suspensions. *Inhalation Toxicology*, **21**, 327-336.
- **Ferris, F.G., Beveridge, T.J.** and **Fyfe, W.S.** (1986) Iron-silica crystallite nucleation by bacteria in a geothermal sediment. *Nature*, **320**, 609-611.
- **Flügel, E.** (2004) Microfacies of Carbonate Rocks. Analysis, Interpretation and Application. Springer-Verlag, 976 pp.
- **Fofonoff, N.P.** (1985) Physical properties of seawater: a new salinity scale and equation of state for seawater. *Journal of Geophysical Research*, **90**, 3332-3342.
- **Gebelein, C.D.** (1974) Guidebook for modern Bahamian platform environments. *GSA Annual Meeting Field Guide*. Boulder, Colorado, USA, 93 pp.
- Glunk, C., Dupraz, C., Braissant, O., Gallagher, K.L., Verrecchia, E.P. and Visscher, P.T. (2011) Microbially mediated carbonate precipitation in a hypersaline lake, Big Pond (Eleuthera, Bahamas). *Sedimentology*, **58**, 720-738.
- **Gray, N.D.** (2006) The unique role of intracellular calcification in the genus *Achromatium*. *Microbiology Monographs*, **1**, 299–309.
- **Gregg, J.M., Bish, D.L., Kaczmarek, S.E.** and **Machel, H.G.** (2015) Mineralogy, nucleation and growth of dolomite in the laboratory and sedimentary environment: a review. *Sedimentology*, **62**, 1749-1769.

- **Griffin W.** (2013) The quest for extraterrestrial life: what about viruses? *Astrobiology*, **13**, 774–783.
- **Grotzinger, J.P.** and **Knoll, A.H.** (1999) Stromatolites in Precambrian carbonates: evolutionary mileposts or environmental dipsticks? *Annual Review of Earth and Planetary Sciences*, **27**, 313-358.
- **Hofmann, H.J., Grey, K., Hickman, A.H.** and **Thorpe, R.J.** (1999) Origin of 3.45 Ga coniform stromatolites in Warrawoona Group, Western Australia. *Geological Society of America Bulletin*, **11**, 1256-1262.
- **Illing, L.V., Wells, A.J.** and **Taylor, J.C.M.** (1965). Penecontemporary dolomite in the Persian Gulf. *SEPM Special Publications*, **13**, 89–111.
- **Jaquet, J.M., Nirel, P.** and **Martignier, A.** (2013) Preliminary investigations on picoplankton-related precipitation of alkaline-earth metal carbonates in meso-oligotrophic Lake Geneva (Switzerland). *Journal of Limnology*, **72**, 592–605.
- **Jones, B.** and **Peng, X.** (2014) Signatures of biologically influenced CaCO<sub>3</sub> and Mg-Fe silicate precipitation in hot springs: case study from Ruidian geothermal area, western Yunnan Province, China. *Sedimentology*, **61**, 56-89.
- **Kaczmarek, S.E., Gregg, J.M., Machel, H.G., Fouke, B.W.** and **Bish, D.L.** (2017) Dolomite, very high-magnesium calcite, and microbes implications for the microbial model of dolomitization. *SEPM Special Publications*, **109**, DOI: http://dx.doi.org/10.2110/sepmsp.109.01
- Kempe, S., Kaźmierczak, J., Landmann, G., Konuk, T., Reimer, A. and Lipp, A. (1991) Largest known microbialites discovered in Lake Van, Turkey. *Nature* **349**, 605–608.
- **Kennard, J.** and **James, N.P.** (1986) Thrombolites and stromatolites: two distinct types of microbial structures. *Palaios*, **1**, 492-503.
- **Köhler, B., Singer, A.** and **Stoffers, P.** (1994) Biogenic nontronite from marine white smoker chimneys. *Clays and Clay Minerals*, **42**, 689-701.
- **Konhauser, K.O.** (1997) Bacterial iron biomineralization in nature. *FEMS Microbiology Reviews*, **20**, 315-326.
- **Konhauser, K.O.** and **Urrutia, M.M.** (1999) Bacterial clay authigenesis: a common biogeochemical process. *Chemical Geology*, **161**, 399-413.
- Konhauser, K.O. (2007) Introduction to Geomicrobiology. Oxford, Blackwell, 440 pp.
- Krause, S., Liebetrau, V., Gorb, S., Sánchez-Roman, M., McKenzie, J.A. and Treude, T. (2012) Microbial nucleation of Mg-rich dolomite in exopolymeric substances under anoxic modern seawater salinity: new insight into an old enigma. *Geology*, **40**, 587-590.
- Kremer, B., Kaźmierczak, J. and Stal, L.J. (2008) Calcium carbonate precipitation in cyanobacterial mats from sandy tidal flats of the North Sea. *Geobiology*, **6**, 46-56.
- **Kyle, J.E., Eydal, H.S.C., Ferris, F.G.** and **Pedersen, K.** (2008a) Viruses in granitic groundwater from 69 to 450m depth of the Aspo hard rock laboratory, Sweden. *The ISME Journal*, **2**, 571–574.
- **Kyle, J.E., Pedersen, K.** and **Ferris, F.G.** (2008b) Virus mineralization at low pH in the Rio Tinto, Spain. *Geomicrobiology Journal*, **25**, 338–345.
- **Laidler J.R.** and **Stedman, K.M.** (2010) Virus silicification under simulated hot spring conditions. *Astrobiology*, **10**, 569–576.
- Léveillé, R.J., Fyfe, W.S. and Longstaffe, F.J. (2000a) An unusual occurrence of Ca-Mg-carbonate-silicate speleothems in basaltic caves, Kauai, Hawaii. *Journal of Geology*, **108**, 613–621.
- **Léveillé**, **R.J.**, **Fyfe**, **W.S.** and **Longstaffe**, **F.J.** (2000b) Geomicrobiology of carbonatesilicate microbialites from Hawaiian basaltic sea caves. *Chemical Geology*, **169**, 339–355.

- **Léveillé, R.J., Longstaffe, F.J.** and **Fyfe, W.S.** (2002) Kerolite in carbonate-rich speleothems and microbial deposits from basaltic sea caves, Kauai, Hawaii. *Clays and Clay Minerals*, **50**, 514–524
- **Léveillé, R.J., Longstaffe, F.J.** and **Fyfe, W.S.** (2007) An isotopic and geochemical study of carbonate-clay mineralization in basaltic caves: abiotic versus microbial processes. *Geobiology*, **5**, 235–249.
- Li, J., Oliver, I. M., Cam, N., Boudier, T., Blondeau, M., Leroy, E. and Benzerara, K. (2016) Biomineralization patterns of intracellular carbonatogenesis in cyanobacteria: molecular hypothesis. *Minerals*, **6**, 10.
- **López-García, P., Kaźmierczak, J., Benzerara, K., Kempe, S., Guyot, F.** and **Moreira, D.** (2005) Bacterial diversity and carbonate precipitation in the giant microbialites from the highly alkaline Lake Van, Turkey. *Extremophiles*, **9**, 263–274.
- Ludwig, R., Al-Horani, F.A., De Beer, D. and Jonkers, H.M. (2005) Photosynthesis-controlled calcification in a hypersaline microbial mat. *Limnology and Oceanography*, **50**, 1836-1843.
- Lyons, W.B., Long, D.T., Hines, M.E., Guadette, H.E. and Armstrong, P.B. (1984) Calcification of cyanobacterial mats in Solar Lake, Sinai. *Geology*, **12**, 623-626.
- **Macintyre, I.G.** (1985) Submarine cements the peloidal question. *SEPM Special Publications*, **36**, 109-116.
- **Manzo**, E., Perri, E. and Tucker, M.E. (2012) Carbonate deposition in a fluvial tufa system: processes and products (Corvino Valley southern Italy). *Sedimentology*, **59**, 553-577.
- Martignier, A., Pacton, M., Filella, M., Jaquet, J.-M., Barja, F., Pollok, K., Langenhorst, F.,
- Lavigne, S., Guagliardo, P., Kilburn, M.R., Thomas, C., Martini, R. and Aritzegui, D. (2017) Intracellular amorphous carbonates uncover a new biomineralization process in eukaryotes. *Geobiology*, **15**, 240-253.
- McKee, E.D. and Gutschick, R.C. (1969) History of the Redwall Limestone of northern Arizona. *GSA Memoirs*, **114**, 1-700.
- Mettraux, M., Homewood, P.W., Al Balushi, S., Erthal, M. and Matsuda, N. (2014) Microbialites of Qarn Alam, Sultanate of Oman. *GeoArabia*, **19**, 17-76.
- **Monty, C.L.V.** (1976) The origin and development of cryptalgal fabric. In: *Stromatolites* (Ed. M.R. Walter), pp. 193-205. Elsevier, Amsterdam.
- **Niederberger, M.** and **Cölfen, H.** (2006) Oriented attachment and mesocrystals: non-classical crystallization mechanisms based on nanoparticle assembly. *Physical Chemistry Chemical Physics*, **8**, 3271-3287.
- Nutman, A.P., Bennett, V.C., Friend, C.R.L., Van Kranendonk, M.J. and Chivas, A.R. (2016) Rapid emergence of life shown by discovery of 3,700-million-year-old microbial structures. *Nature*, **537**, 535-538.
- Orange, F., Chabin, A., Gorlas, A., Lucas-Staat, S., Geslin, C., Le Romancer, M., Prangishvili, D., Forterre, P. and Westall, F. (2011) Experimental fossilisation of viruses from extremophilic Archaea. *Biogeosciences*, **8**, 1465–1475.
- Pace, A., Bourillot, R., Bouton, A., Vennin E., Galaup, S., Bundeleva, I., Patrier, P., Dupraz, C., Thomazo, C., Sansjofre, P., Yokoyama, Y., Franceschi, M., Anguy, Y., Pigot, L., Virgone, A. and Visscher, P.T. (2016) Microbial and diagenetic steps leading to the mineralisation of Great Salt Lake microbialites. *Scientific Reports*, 6, 31495.
- Pacton, M., Wacey, D., Corinaldesi, C., Tangherlini, M., Kilburn, M.R., Gorin, G., Danovaro, R. and Vasconcelos, C. (2014) Viruses as new agents of organomineralization in the geological record. *Nature Communications*, 5, 4298.
- Pacton, M., Sorrel, P., Bevillard, B., Zacaï, A., Vinçon-Laugier, A. and Oberhänsli, H. (2015) Sedimentary facies analyses from nano- to millimetre scale exploring past microbial

- activity in a high-altitude lake (Lake Son Kul, Central Asia). *Geological Magazine*, **152**, 902–922.
- **Paerl, H.W., Steppe, T.F.** and **Reid, R.P.** (2001) Bacterially mediated precipitation in marine stromatolites. *Environmental Microbiology*, **3**, 123-130.
- **Parkhurst, D.L.** and **Appelo, C.A.J.** (2013) Description of input and examples for PHREEQC version 3 a computer program for speciation, batch-reaction, one-dimensional transport, and inverse geochemical calculations. *USGS Techniques and Methods*, **6**, 497 pp.
- **Paulo, C.** and **Dittrich, M.** (2013) 2D Raman spectroscopy study of dolomite and cyanobacterial extracellular polymeric substances from Khor Al-Adaid sabkha (Qatar). *Journal of Raman Spectroscopy*, **44**, 1563-1569.
- **Peng, X., Xu, H., Jones, B., Chen, S.** and **Zhou, H.** (2013) Silicified virus-like nanoparticles in an extreme thermal environment: implications for the preservation of viruses in the geological record. *Geobiology*, **11**, 511–526.
- **Perri, E.** and **Tucker, M.E.** (2007) Bacterial fossils and microbial dolomite in Triassic stromatolites. *Geology*, **35**, 207-210.
- **Perri, E.** and **Spadafora, A.** (2011) Evidence of microbial biomineralization in modern and ancient stromatolites. In: Stromatolites: Interaction of Microbes with Sediments (Eds V. Tewari and J. Seckbach), *Cellular Origin, Life in Extreme Habitats and Astrobiology,* **18**, 631-649.
- **Perri, E., Tucker, M.E.** and **Spadafora, A.** (2012a) Carbonate organo-mineral micro- and ultrastructures in sub-fossil stromatolites: Marion Lake, South Australia. *Geobiology*, **10**, 105-117.
- **Perri, E., Manzo, E.** and **Tucker, M.E.** (2012b) Multi-scale study of the role of the biofilm in the formation of minerals and fabrics in calcareous tufa. *Sedimentary Geology*, **263**, 16-29.
- **Reitner, J.** and **Neuweiler, F.** (1995) Mud mounds: a polygenetic spectrum of fine-grained carbonate buildups. *Facies*, **32**, 1-69.
- **Riding, R.** (2000) Microbial carbonates: the geological record of calcified bacterial-algal mats and biofilms. *Sedimentology*, **47**, 179-214.
- **Riding, R.** (2002a) Structure and composition of organic reefs and carbonate mud mounds: concepts and categories. *Earth-Science Reviews*, **58**, 163-231.
- **Riding, R.** (2002b) Biofilm architecture of Phanerozoic cryptic carbonate marine veneers. *Geology*, **30**, 31-34.
- **Riding, R.** and **Tomás, S.** (2006) Stromatolite reef crusts, Early Cretaceous, Spain: bacterial origin of in situ precipitated peloid microspar? *Sedimentology*, **53**, 23-34.
- Rodriguez-Blanco, J.D., Shaw, S. and Benning, L.G. (2015) A route for the direct crystallization of dolomite. *American Mineralogist*, **100**, 1172–1181.
- **Sánchez-Navas, A., López-Cruz, O., Velilla, N.** and **Vidal, I.** (2013) Crystal growth of lead carbonates: influence of the medium and relationship between structure and habit. *Journal of Crystal Growth*, **376**, 1-10.
- Sánchez-Román, M., Vasconcelos, C., Schmid, T., Dittrich, M., McKenzie, J.A., Zenobi, R. and Rivadeneyra, M.A. (2008) Aerobic microbial dolomite at the nanometer scale: implications for the geologic record. *Geology*, **36**, 879-882.
- Sánchez-Román, M., Vasconcelos, C., Warthmann, R., Rivadeneyra, M. and McKenzie, J.A. (2009) Microbial dolomite precipitation under aerobic conditions: results from Brejo do Espinho Lagoon (Brazil) and culture experiments. *IAS Special Publications*, **41**, 167–178.
- Sánchez-Román, M., Romanek, C.S., Fernández-Remolar, D.C., Sánchez-Navas, A., McKenzie, J.A., Pibernat, R.A. and Vasconcelos, C. (2011) Aerobic biomineralization of Mg-rich carbonates: Implications for natural environments. *Chemical Geology*, **281**, 143-150. Słowakiewicz, M., Pancost, R.D., Thomas, L., Tucker, M.E., Ooi, S.M.D. and Whitaker,
- **F.** (2014) Holocene intertidal microbial mats of Qatar and their implications for petroleum

- source rock formation in carbonate-siliciclastic-evaporite systems. *International Petroleum Technology Conference*, 19-22 January, Doha, Qatar, IPTC-17400-MS.
- **Slowakiewicz, M., Whitaker, F., Thomas, L., Tucker, M.E., Zheng, Y., Gedl, P.** and **Pancost, R.D.** (2016) Biogeochemistry of intertidal microbial mats from Qatar: new insights from organic matter characterisation. *Organic Geochemistry*, **102**, 14-29.
- **Souza-Egipsy, V., Wierzchos, J., Ascaso, C.** and **Nealson, K.H.** (2005) Mg-silica precipitation in fossilization mechanisms of sand tufa endolithic microbial community, Mono Lake (California). *Chemical Geology*, **217**, 77–87.
- **Spadofora, A., Perri, E., McKenzie, J.A.** and **Vasconcelos, C.** (2010) Microbial biomineralization processes forming modern Ca:Mg carbonate stromatolites. *Sedimentology*, **57**, 27-40.
- **Staudt, C., Horn, H., Hempel, D.C.** and **Neu, T.R.** (2004) Volumetric measurements of bacterial cells and extracellular polymeric substance glycoconjugates in biofilms. *Biotechnology and Bioengineering*, **88**, 585-592.
- **Strohmenger, C.J.** and **Jameson, J.** (2015) Modern coastal systems of Qatar as analogues for arid climate carbonate reservoirs: improving geological and reservoir modelling. *First Break*, **33**, 41-50.
- **Sutherland, I.A.** (2001) Exopolysaccharides in biofilms, floc and related structures. *Water Science and Technology*, **43**, 77–86.
- **Suttle, C.A.** (2007) Marine viruses major players in the global ecosystem. *Nature Reviews in Microbiology*, **5**, 801–812.
- **Suttle, C.A.** (2013) Viruses: unlocking the greatest biodiversity on Earth. *Genome*, **56**, 542–544.
- **Tazaki, K.** (1997) Biomineralization of layer silicates and hydrated Fe/Mn oxides in microbial mats: an electron microscopical study. *Clays and Clay Minerals*, **45**, 203-212.
- **Tazaki, K.** (2007) Clays, microorganisms, and biomineralization. In: *Handbook of Clay Science* (Eds F. Bergaya, B.K.G. Theng and G. Lagaly). The Netherlands, Elsevier, 1224 pp.
- **Thompson, J.B.** and **Ferris, F.G.** (1990) Cyanobacterial precipitation of gypsum, calcite, and magnesite form natural alkaline lake water. *Geology*, **18**, 995-998.
- **Ueshima, M.** and **Tazaki, K.** (2001) Possible role of microbial polysaccharides in nontronite formation. *Clays and Clay Minerals*, **49**, 292-299.
- **Urrutia**, **M.M.** and **Beveridge**, **T.J.** (1993) Mechanism of silicate binding to the bacterial cell wall in *Bacillus subtilis*. *Journal of Bacteriology*, **175**, 1936-1945.
- **Urrutia, M.M.** and **Beveridge, T.J.** (1994) Formation of fine-grained metal and silicate precipitates on a bacterial surface (*Bacillus subtilis*). *Chemical Geology*, **116**, 261-280.
- **Urrutia, M.M.** and **Beveridge, T.J.** (1995) Formation of short-range ordered aluminosilicates in the presence of a bacterial surface (*Bacillus subtilis*) and organic ligands. *Geoderma*, **65**, 149-165.
- **Vasconcelos, C., McKenzie, J.A., Bernasconi, S., Grujic, D.** and **Tien, A.** (1995) Microbial mediation as a mechanism for natural dolomite formation at low temperatures. *Nature*, **377**, 220-222.
- Vasconcelos, C., Warthmann, R., McKenzie, J.A., Visscher, P.T., Bittermann, A.G. and van Lith, Y. (2006) Lithifying microbial mats in Lagoa Vermelha, Brazil: modern Precambrian relics? *Sedimentary Geology*, 18, 175-183.
- Van Kranendonk, M.J., Philippot, P., Lepot, K., Bodorkos, S. and Pirajno, F. (2008) Geological setting of Earth's oldest fossils in the c. 3.5 Ga Dresser Formation, Pilbara craton, Western Australia. *Precambrian Research*, **167**, 93-124.
- Visscher, P.T., Reid, R.P., Bebout, B.M., Hoeft, S.E., Macintyre, I.G. and Thompson, Jr., J. (1998) Formation of lithified micritic laminae in modern marine stromatolites (Bahamas): the role of sulfur cycling. *American Mineralogist*, **83**, 1482–1491.

- Warthmann, R., Vasconcelos, C., Sass, H. and McKenzie, J.A. (2005) *Desulfovibrio brasiliensis* sp. nov., a moderate halophilic sulfate-reducing bacterium from Lagoa Vermelha (Brazil) mediating dolomite formation. *Extremophiles*, **9**, 255–261.
- Whitaker, F., Ooi, S.M.D., Jameson, J. and Strohmenger, C.J. (2014) Origins of evaporites in a Holocene mixed clastic and carbonate coastal sabkha: preliminary hydrological and geochemical data from Mesaieed sabkha, Qatar. *International Petroleum Technology Conference*, 19-22 January, Doha, Qatar, IPTC-17567-MS.
- **Wingender, J., Neu, T.R.** and **Flemming, H.-C.** (1999). Microbial extracellular polymeric substances; characterization, structure, and function. Berlin, Springer, 258 p.
- **Wong, H.L., Smith, D.-L., Visscher, P.T.** and **Burns, B.P.** (2015) Niche differentiation of bacterial communities at a millimeter scale in Shark Bay microbial mats. *Scientific Reports*, **5**, 15607.
- Yeates, T.O., Kerfeld, C.A., Heinhorst, S., Cannon, G.C. and Shively, J.M. (2008) Protein-based organelles in bacteria: carboxysomes and related microcompartments. *Nature Reviews Microbiology*, **6**, 681-691.
- Zeyen, N., Benzerara, K., Li, J., Groleau, A., Balan, E., Robert, J.-L., Estève I., Tavera, R., Moreira, D. and López-García, P. (2015) Formation of low-T hydrated silicates in modern microbialites from Mexico and implications for microbial fossilization. *Frontiers in Earth Science*, **3**, 64.
- **Zhang, F., Xu, H., Konishi, H., Shelobolina, E.S.** and **Roden, E.E.** (2012a) Polysaccharide-catalyzed nucleation and growth of disordered dolomite: a potential precursor for sedimentary dolomite. *American Mineralogist*, **97**, 556–567.
- **Zhang, F., Xu, H., Konishi, H., Kemp, J.M., Roden, E.E.** and **Shen, Z.** (2012b) Dissolved sulfide-catalyzed precipitation of disordered dolomite: implications for the formation mechanism of sedimentary dolomite. *Geochimica et Cosmochimica Acta*, **97**, 148–165.

#### **CAPTIONS TO FIGURES**

- **Fig. 1.** Google Earth image and details of microbial mats in the northern part of Mesaieed. (A) Google Earth image (from 2013) of the Mesaieed area showing narrow intertidal lagoons, elongate parallel to the coastline and connected with the sea via narrow inlets. Lagoons are fringed by bands of mangrove and chenier beach. (B) Desiccated microbial mats (N 25°3'3.29" E 51°36'41.82") and a mangrove and chenier beach belt in the distance (all pictures taken in 2014). (C) Detail of (B) showing desiccated and deformed mats into saucershaped polygons and *Avicennia* mangroves in the distance. (D) Detail of (C) showing edges of mat polygons which are upturned and darker in colour.
- **Fig. 2.** Microbiological profile of the mat (N 25°3'3.29" E 51°36'41.82") with sampling intervals: circles = pore water chemistry; squares = bulk chemistry. Note that detailed microbiological and molecular studies of the mat were presented in Al-Thani *et al.* (2014) and Słowakiewicz *et al.* (2016).
- **Fig. 3.** Mesaieed mat hydrochemical parameters; salinity, temperature, pH and dissolved O<sub>2</sub> measured *in situ*; and <sub>p</sub>CO<sub>2</sub> and saturation index (SI) with respect to aragonite, calcite, dolomite and gypsum.
- **Fig. 4.** (A) Typical scanning electron microscopy (SEM) view of the mat with bacterial forms (dark arrow) and minerals (dashed arrows) enveloped within a thick layer of extracellular polymeric substances (EPS; white arrows). (B) Same field as (A) but with back-scattered electrons (BSE) in which organic matter (EPS and bacteria) are almost transparent and minerals appear brighter. (C) Tubular sheaths of EPS (dark arrow) covering cyanobacterial chains of cells; some are empty (white arrow). (D) Transmission electron microscopy (TEM) picture of a bacterial cell surrounded by EPS (white arrow), which appears as a filamentous network of randomly coiled polymeric chains extending from the cell membrane. EPS are partially mineralized (electron-dense, darker zones).
- **Fig. 5.** Neo-formed minerals closely associated with micro-organisms inhabiting the mat and in continuity with them. (A) Extracellular polymeric substances (EPS; white arrows) making a transition to neo-formed minerals (dashed arrows); note living bacterial cells (black arrow). (B) Back-scattered electron (BSE) view of the same field in (A). (C) EPS (white arrow) making a transition to neo-formed minerals (dashed arrow). Bacterial cells are also mineralized (dark arrow). (D) BSE picture of the same field as (A).
- **Fig. 6.** (A) and (B) Early stage of mineral formation showing that the initial sites of mineral nucleation (dashed arrow), and accretion, are almost exclusively within the extracellular polymeric substances (EPS; white arrow) that surround the bacterial cells (dark arrow). (B) Same field as (A) but with back-scattered electrons (BSE). (C) and (D) Transmission electron microscopy (TEM) views of the same process illustrated in (A) with scanning electron microscopy (SEM); the EPS (white arrows) are the initial site of mineral nucleation (electron-

dense, darker areas, dashed arrows). Note that the interstitial fluid between the microorganisms lacks any type of neo-formed minerals.

- **Fig. 7.** (A) and (B) Close-up transmission electron microscopy (TEM) views of extracellular polymeric substances (EPS) in which inorganic nanoparticles (electron-dense, darker spots, dashed arrows) appear along the threads that compose the EPS (white arrow) and gradually aggregate to form larger masses. (C) Scanning electron microscopy (SEM) view of nanoparticles mineralizing EPS and forming larger masses irregular to sub-spherical in shape (dashed arrows). Note bacterial cells (dark arrows). (D) Back-scattered electron (BSE) view of same field as (C) in which the inorganic denser compounds are lighter and more easily distinguished from organic matter.
- **Fig. 8.** Elemental compositional maps of mineralizing extracellular polymeric substances (EPS). Maps show the accumulation of cations in the whole EPS, rather than just coinciding with the nanoparticles as is the case for Si and Al in the (B) area. Carbon, oxygen and nitrogen are not shown but are present for 95 to 98% of the total element composition.
- **Fig. 9.** Mineral crystals in mineralized extracellular polymeric substances (EPS). (A) Note the two types of nanocrystal; fibrous and ovoid/irregular. Transmission electron microscopy (TEM) view. (B) Selected area electron diffraction (SAED) of the area in (A) showing a poly-crystalline pattern.
- **Fig. 10.** (A) Section of the mat between 1 mm and 2 mm from the surface. Note the abundance of mineral particles (lighter spots). Scanning electron microscopy back-scattered electron microscopy (SEM BSE) view. (B) Close-up view of the dashed square in (A) in which minerals are present as small spots but also forming larger peloids with irregular to sub-ovoidal shapes. (C) Close-up view of a peloid, the dashed square in (B), in which the carbonate present forms small rhombohedra (white arrow) surrounded by smaller clay minerals (dark arrow). (D) Close-up view of the dashed square in (C), showing both crystal types, particularly the fibrous clay. (E) Another example of a peloid in which the carbonate and the clay are present. (F) Close-up view of the dashed area in (E) in which the carbonate minerals are anhedral (white arrow).
- **Fig. 11.** (A) An example of an aragonitic peloid. Note that the peloids are particularly rich in mineralized bacterial cells (dark arrow) and extracellular polymeric substances (EPS; white arrow), as is clearly visible in the close-up view (B). (C) Calcium-carbonate peloids composed of a cluster of sub-ovoidal crystallites composed of nanocrystals. Scanning electron microscopy back-scattered electron microscopy (SEM BSE) view. (D) Close-up view of the dashed area in (C) showing that each crystallite is enveloped in EPS (white arrow); note also bacteria (dark arrow).
- **Fig. 12.** (A) Cubic pyrite nanocrystals (white squares) associated with ovoid carbonate and clay mineral. Scanning electron microscopy back-scattered electron microscopy (SEM BSE) view. (B) SEM BSE view of the same field in (A) showing that all crystals are

associated with extracellular polymeric substances (EPS). (C) Sub-spherical framboids of pyrite. SEM – BSE view.

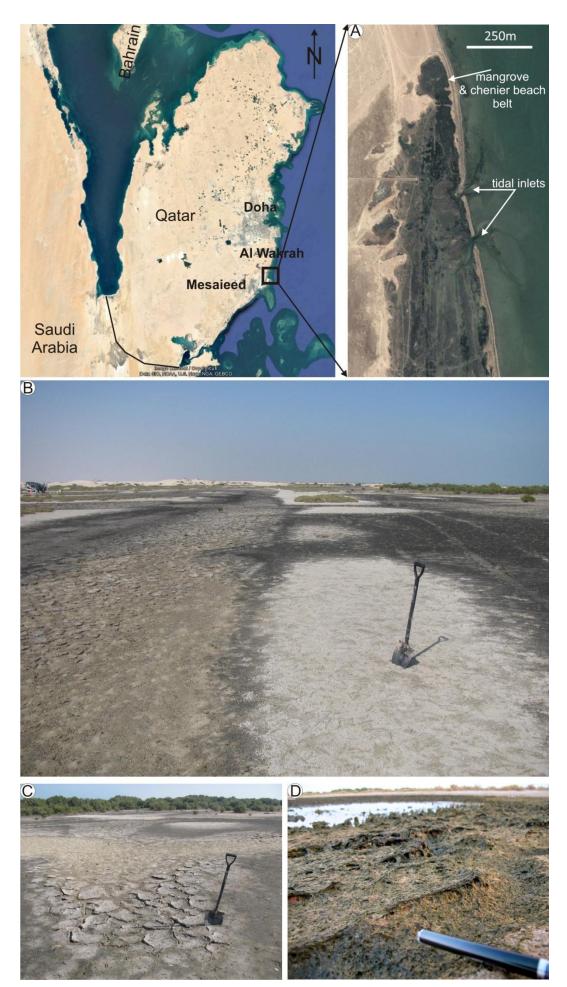
- **Fig. 13.** X-ray diffraction (XRD) of the mineral residue after organic matter removal. (A) Spectrum of all mineral phases. (B) Detailed spectrum for the carbonate phases. Aragonite (A), low-Mg calcite (C), high-Mg calcite (HMgC), very-high-Mg calcite/dolomite (D), quartz (Q), palygorskite (P) and indeterminate clay mineral (Cl).
- **Fig. 14.** (A) Calcite crystallites to the right and 100 nm scale nanospheroids in the foreground and behind. (B) A random collection of calcite crystallite bundles, mostly *ca* 3 μm in length, some clearly triangular in cross-section with a flat top. (C) Cones of calcite crystallites, the central ones of which have nucleated on nanometre-scale particles of amorphous material (dashed white arrow); the fine point of initiation is visible in several 'loose' cones. (D) Calcite crystallite cones [energy-dispersive X-ray spectrometer (EDS) Ca 23.5%, Mg 0.66%] with sharp nucleation points and flat tops, which have nucleated on both sides of a carbonate grain of high-Mg composition (EDS Ca 13.4%, Mg 12.1%). Note the other cones, several with a triangular cross-section and a slightly larger one (dashed arrow) with a termination beginning to develop on the top. (E) A dumb-bell type of arrangement of crystallite cones with hemispherical tops. (F) A densely-packed, but not interfering, near-vertical arrangement of crystallite cones with triangular cross-sections, growing on a substrate of a bioclast fragment.
- **Fig. 15.** (A) and (B) Crystallite cones which are developing a six-sided, hexagonal shape, with a central hole. In (B) a termination is beginning to form on the slightly larger one (dashed arrow). Field of view in (B) is 15 μm across. (C) and (D) Terminations beginning to form on the tops of crystal cones; note the gap where faces have not quite joined and the central hole, triangular in shape, gradually disappearing. (E) Collection of crystals formed from one sharp initiation point with nearly complete terminations. The sub-bundle arrangement of crystallites is still visible on the side view. Note 100 nm scale nanospheroids (dashed arrow). (F) Good crystals have now formed with smooth surfaces and terminations.
- **Fig. 16.** (A) Very high-Mg carbonate crystal (2 μm across) [energy-dispersive X-ray spectrometer (EDS) Ca 3.9%, Mg 4.2%] with a rhombic shape covered in extracellular polymeric substances (EPS; hence EDS gave high C and O). (B) Very high-Mg carbonate crystal (EDS Ca 16.9%, Mg 12.6%) with visible layered structure and small clay fibres on the surface (dashed arrow). (C) Clay fibres with EDS composition Mg 8.5%, Al 1.9%, Si 8.4%, Ca 5.4% O 61.7%. (D) Felted mat of clay fibres with prominent tips at the ends of the fibres. (E) A felted mat of clay fibres with holes (arrow, alveolar structure), which could well be a permineralized sheet of EPS. Note micron-sized rhombic crystal (dashed arrow) which has a high-Mg carbonate content (Mg 10.4%; Ca 8.3%). (F) A collection of Ca-carbonate (low-Mg) crystals (2 to 4 μm long) which have the appearance of aragonite.
- Fig. 17. (A) Large numbers of nanospheres (white arrows), around 50 to 70 nm in diameter occurring in clusters or peloidal aggregates, which are enveloped in extracellular polymeric

substances (EPS; white dashed arrows). A coccoid bacterium, 2 μm in length (black dashed arrow), has a group of viruses attached at the top (black arrow). Dashed rectangle: field of (B). Scanning electron microscopy – back-scattered electron microscopy (SEM – BSE) view from the uppermost green lamina of the microbial mat. (B) Detail of (A) showing viruses attached to a procaryote bacterium and viral-like particles within a cluster. Notice the shape of the VLP; not perfect spheroids, but with flat surfaces and edges. Also note nanospheres appearing to coalesce (in the background). (C) A larger field of view than that in (A) (dashed rectangle is A field) but in BSE mode showing partial permineralization of the viral-like particles and *ca* 2 μm sized clusters (peloids in the making).

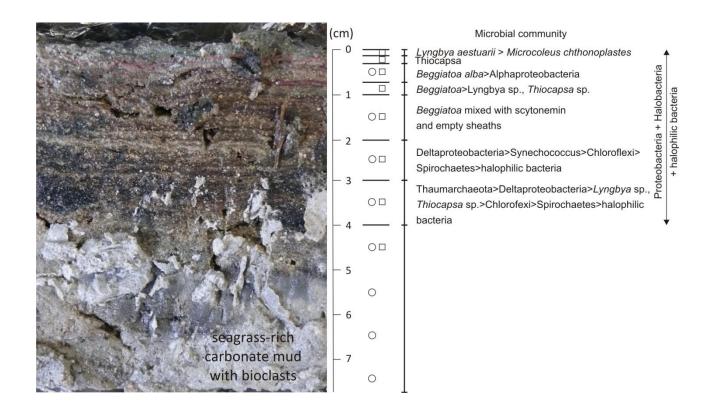
**Fig. 18.** Transmission electron microscopy (TEM) images showing unicellular bacteria with a dark cell wall and a 300 to 500 nm thick coating of extracellular polymeric substances (EPS; black arrows in A and B) showing a dark thread-like texture. The bacterium in (C) (dashed circle) lacks the cell wall. Within the bacteria are numerous nanospheres (dashed black arrows) with a dark outer wall and all a similar size (*ca* 30 to 150 nm), some of them are partially to totally mineralized (dashed white arrows). Energy-dispersive X-ray spectrometer (EDS) analyses of these give the presence of Ca, Mg, S, Si, Al and Fe. These are interpreted as viral-like particles, possibly viruses themselves. Thylakoid structures of dark interconnected membranes (white arrows in A and C) are also present indicating that these are photosynthetic bacteria. Samples from uppermost green layer of the microbial mat. Scale bars = 500 nm.

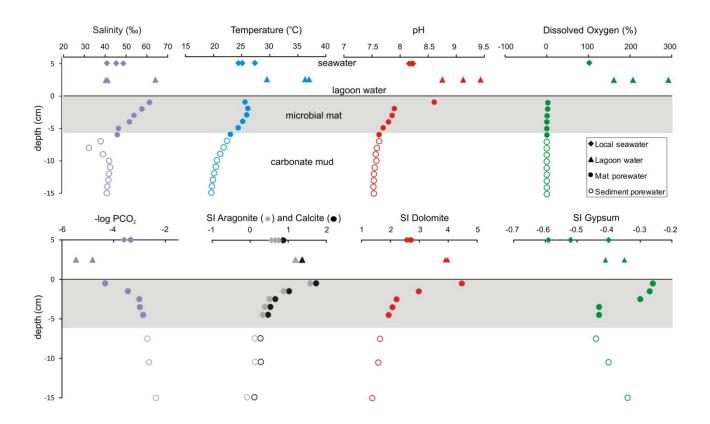
**Fig. 19.** (A) Microspheres showing variable size, 750 nm to 1 μm, and shape, spheroidal but slightly irregular or with flattish sides (arrows). Energy-dispersive X-ray spectrometer (EDS) analysis here gives C 28.9%, Na 1.2%, Mg 1.3%, Si 2.0%, O 65.17%. (B) Microspheroids with a rough surface (arrows) appearing to be composed of tiny crystallites. The average EDS analysis of the three structures here gives C 16.5%, Na 0.7%, Al 2.7%, Si 1.8%, Ca 3.8%, Fe 15.5%, O 59%. (C) Spheroidal structures with smooth surface (arrows) but showing variable size and shape. Some appear to be coalescing into larger structures.

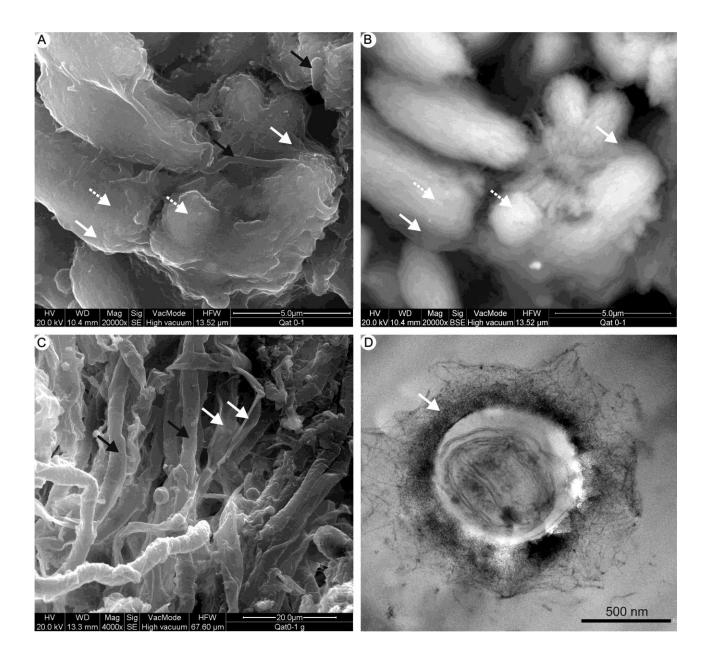
**Fig. 20.** Schematic figure showing the development of calcite crystals from conical bundles of crystallites.

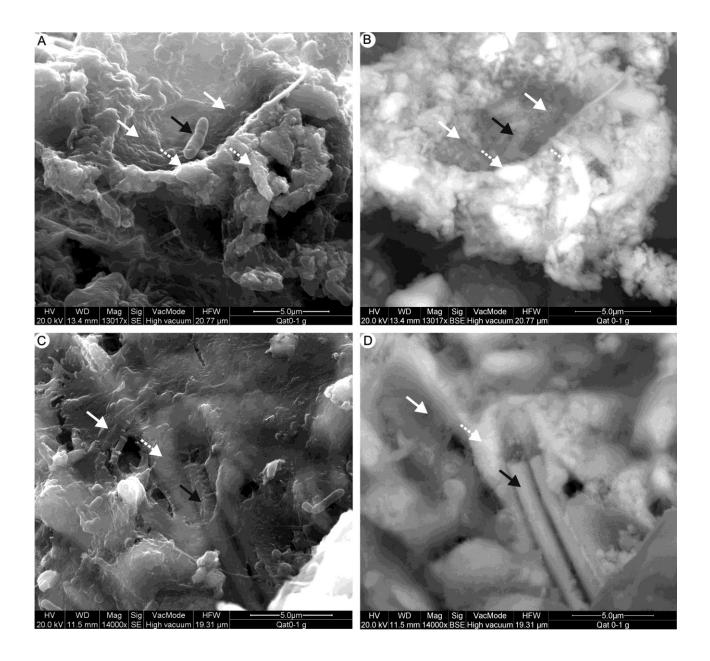


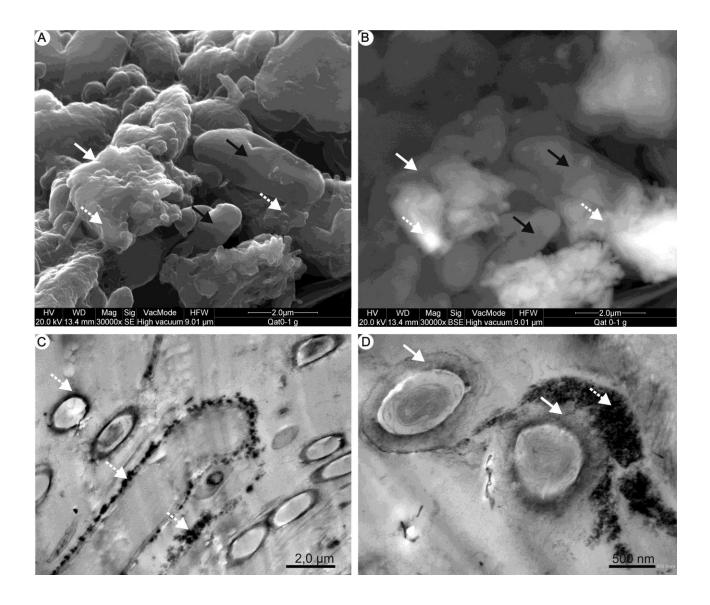
This article is protected by copyright. All rights reserved.

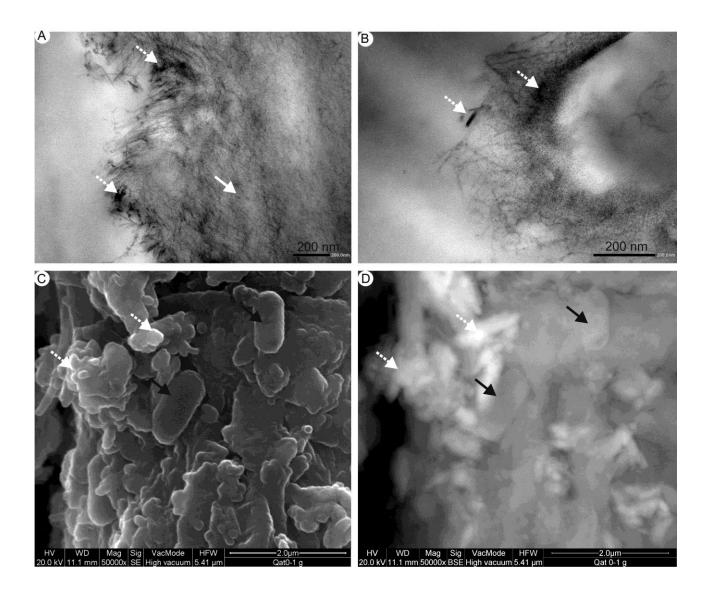


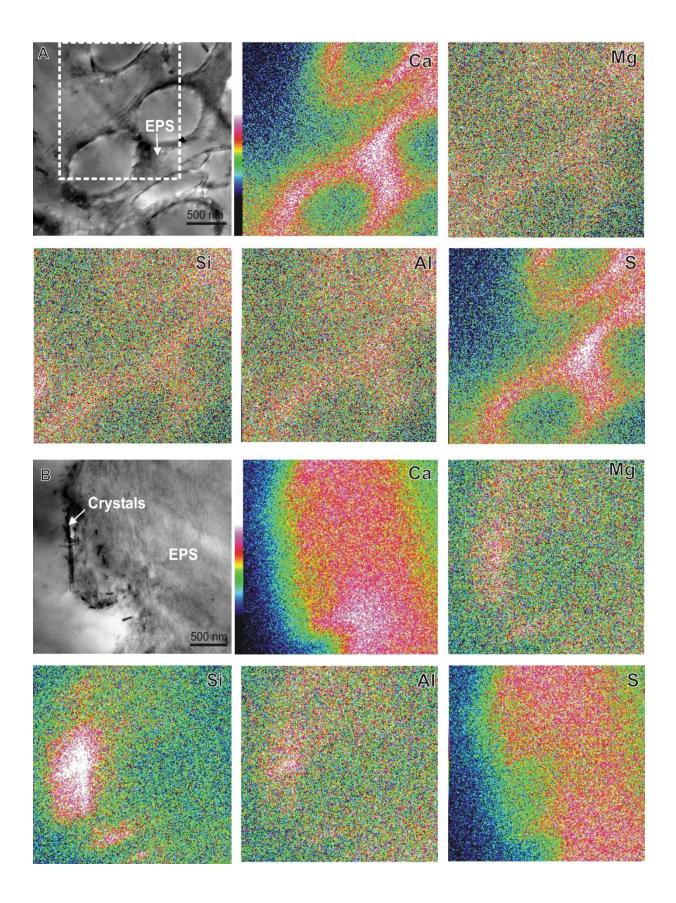


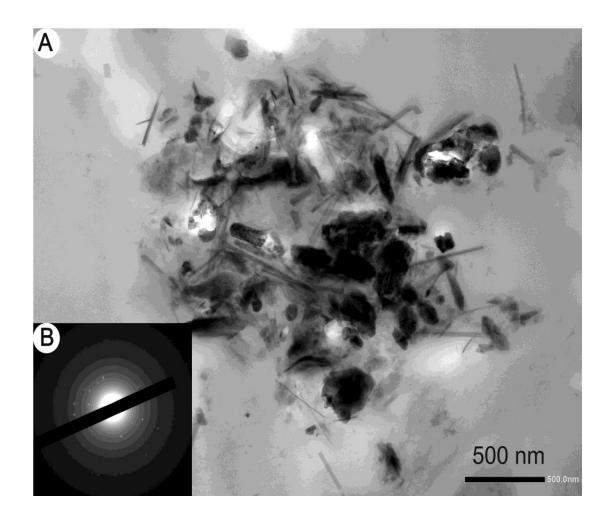


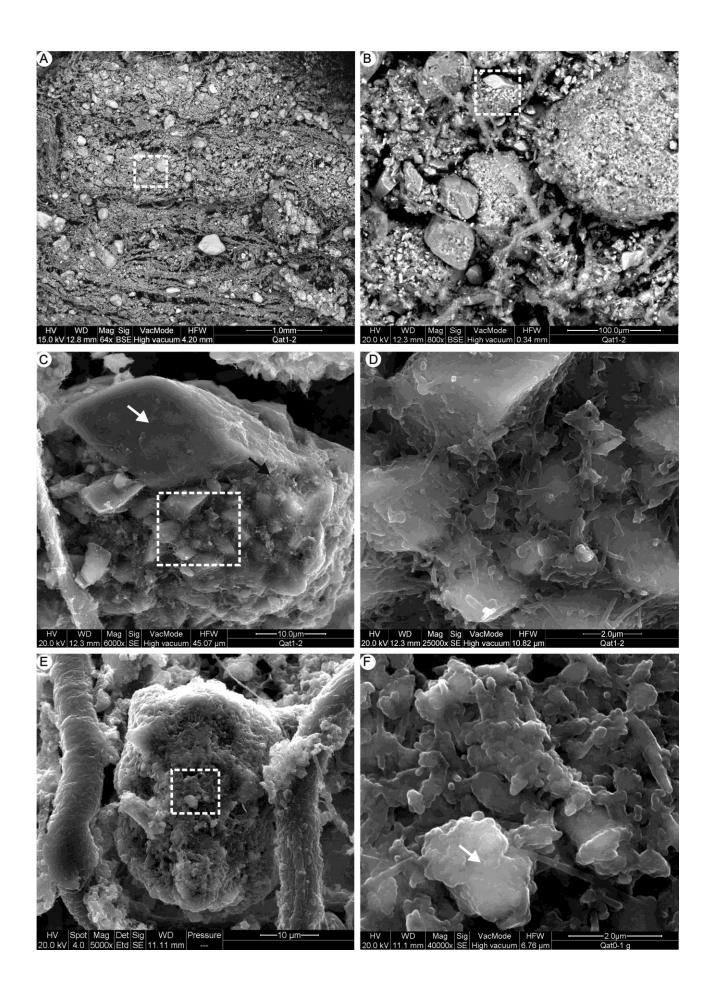




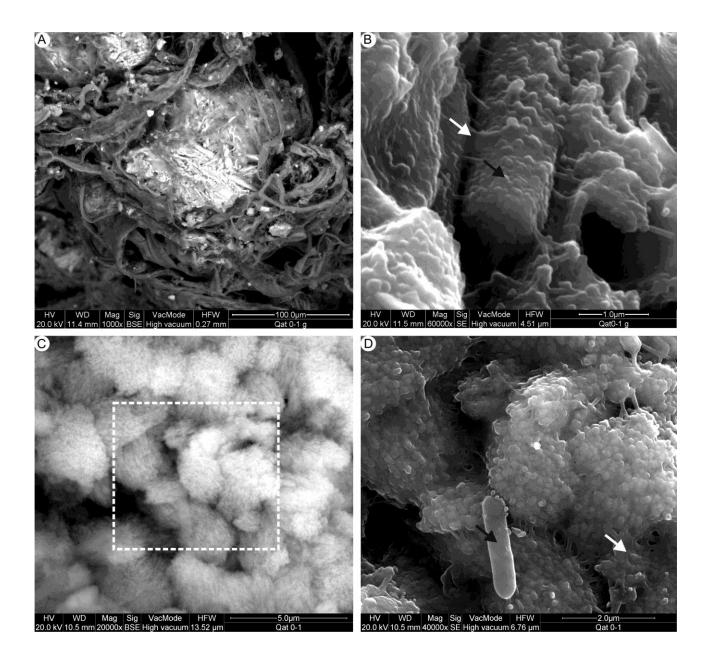


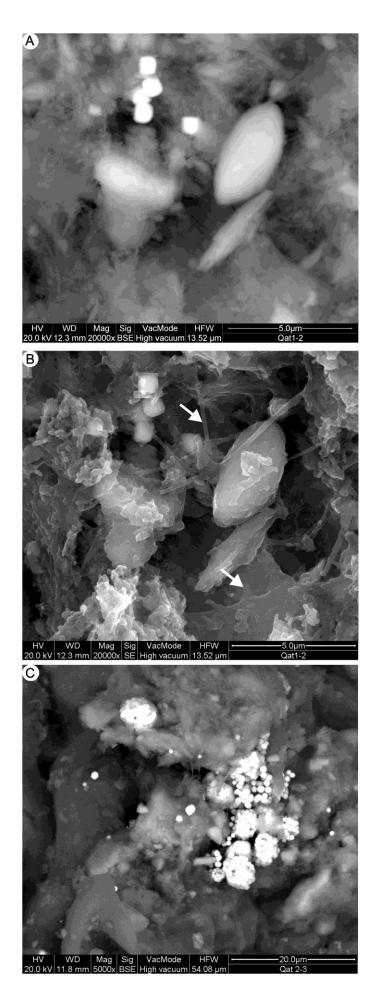




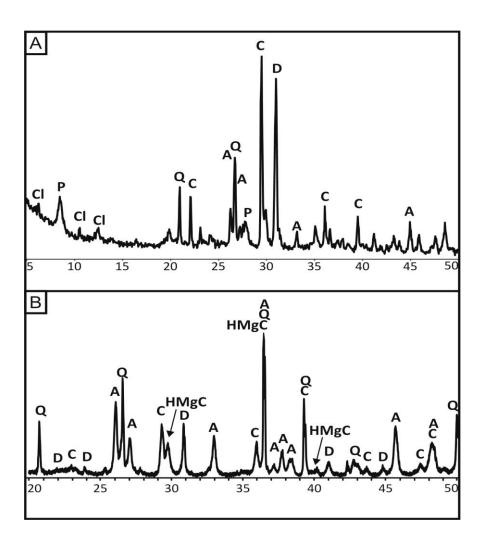


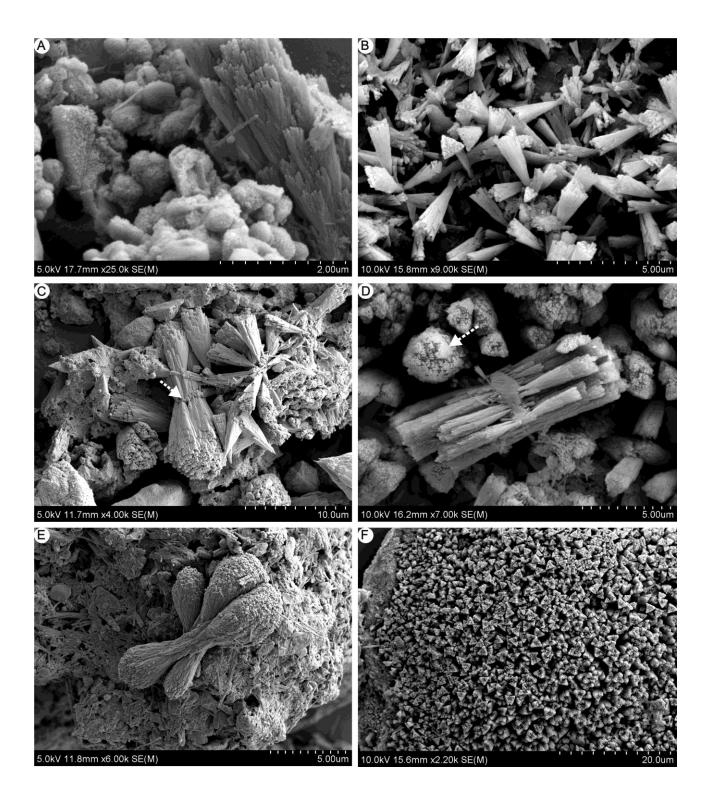
This article is protected by copyright. All rights reserved.

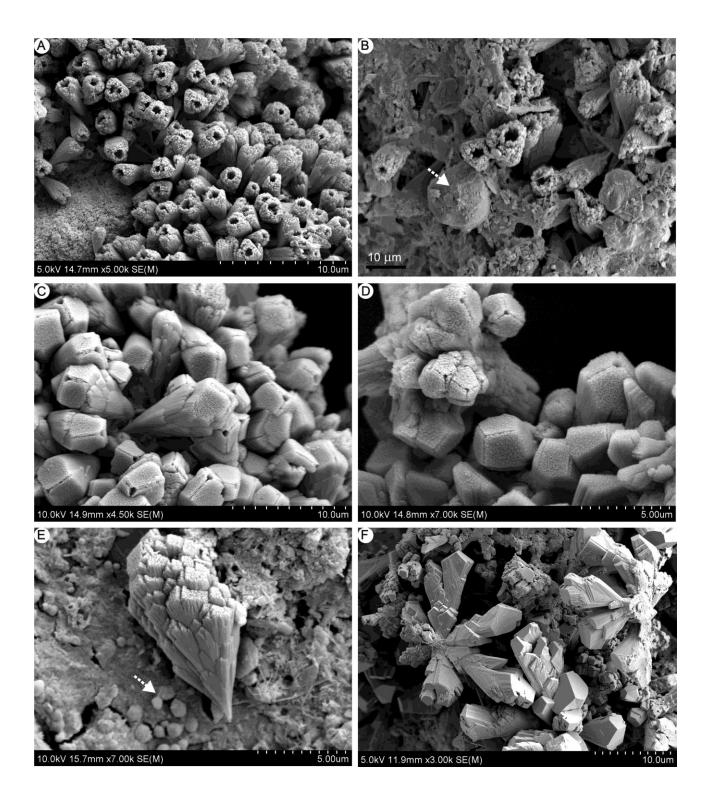


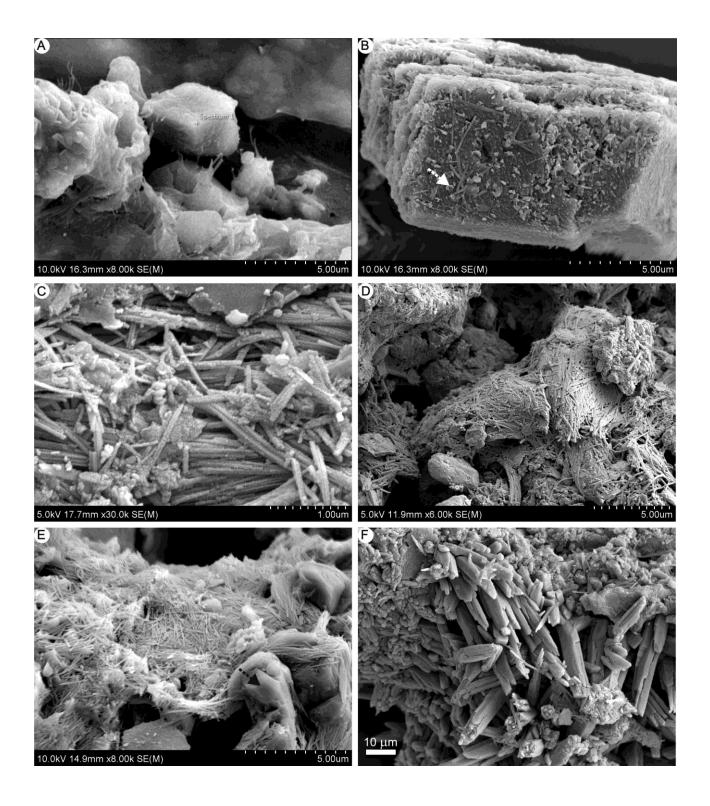


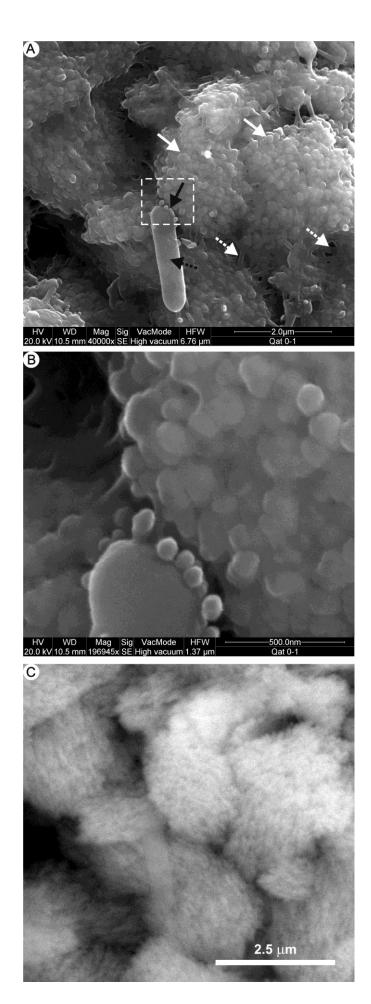
This article is protected by copyright. All rights reserved.











This article is protected by copyright. All rights reserved.

